CORRECTION POSTED 3 MAY 2023

SCIENCE ADVANCES | RESEARCH ARTICLE

NEUROSCIENCE

Prostaglandin EP3 receptor–expressing preoptic neurons bidirectionally control body temperature via tonic GABAergic signaling

Yoshiko Nakamura[1], Takaki Yahiro[1], Akihiro Fukushima[1], Naoya Kataoka[1,2], Hiroyuki Hioki[3], Kazuhiro Nakamura[1]*

The bidirectional controller of the thermoregulatory center in the preoptic area (POA) is unknown. Using rats, here, we identify prostaglandin EP3 receptor–expressing POA neurons (POA^{EP3R} neurons) as a pivotal bidirectional controller in the central thermoregulatory mechanism. POA^{EP3R} neurons are activated in response to elevated ambient temperature but inhibited by prostaglandin E_2, a pyrogenic mediator. Chemogenetic stimulation of POA^{EP3R} neurons at room temperature reduces body temperature by enhancing heat dissipation, whereas inhibition of them elicits hyperthermia involving brown fat thermogenesis, mimicking fever. POA^{EP3R} neurons innervate sympathoexcitatory neurons in the dorsomedial hypothalamus (DMH) via tonic (ceaseless) inhibitory signaling. Although many POA^{EP3R} neuronal cell bodies express a glutamatergic messenger RNA marker, their axons in the DMH predominantly release γ-aminobutyric acid (GABA), and their GABAergic terminals are increased by chronic heat exposure. These findings demonstrate that tonic GABAergic inhibitory signaling from POA^{EP3R} neurons is a fundamental determinant of body temperature for thermal homeostasis and fever.

INTRODUCTION

Thermoregulation is a physiological function fundamental to homeostasis in mammals. Body core temperature is maintained within a control range by autonomous regulation of the balance between heat production within the body and heat loss to the environment. Autonomic thermoregulatory responses, such as sympathetic thermogenesis in brown adipose tissue (BAT) and heat loss control through skin vasomotion, are governed by the central nervous system. The central regulation of autonomic thermoregulatory responses is mediated by the thermoregulatory center in the preoptic area (POA) of the hypothalamus and the sympathoexcitatory efferent pathways involving the dorsomedial hypothalamus (DMH) and rostral medullary raphe region (rMR) (*1*–*4*). However, the principle of the mechanism by which the POA thermoregulatory center controls the sympathoexcitatory pathways remains to be elucidated.

The POA receives and integrates thermosensory (cool- and warm-sensory) neural signals from skin thermoreceptors and a pyrogenic humoral signal mediated by prostaglandin E_2 (PGE_2), which is produced in response to infections (*5*–*7*). The POA has been postulated to provide strong tonic (ceaseless) inhibitory influences to sympathoexcitatory neurons in the DMH and rMR to regulate the tones of sympathetic outflows to thermoregulatory effectors, because a knife cut to disrupt descending fibers from the POA causes dysregulated increases in BAT thermogenesis and cutaneous vasoconstrictor activity leading to lethal hyperthermia (*8*, *9*). These findings suggest that the descending tonic inhibition from the POA, whose intensity is altered by thermosensory and pyrogenic afferent signals, is a fundamental determinant of body temperature. However, the POA neurons that provide this descending tonic inhibitory signaling to bidirectionally control body temperature have yet to be identified.

A group of POA neurons that express the EP3 subtype of PGE receptors (EP3Rs; POA^{EP3R} neurons) has been hypothesized to provide the tonic inhibition (*3*, *10*, *11*), as supported by the anatomical observation that the POA^{EP3R} neuron group includes γ-aminobutyric acidergic (GABAergic) inhibitory neurons and projects to the DMH and rMR (*10*, *12*, *13*). EP3R proteins are localized in neuronal cell bodies and dendritic fibers in the median preoptic nucleus (MnPO) and medial POA (MPA) (fig. S1, A and B) (*14*, *15*) and mediate the febrile action of PGE_2 (*16*). However, there is no evidence that POA^{EP3R} neurons are involved in basal thermoregulation. This is because no study has manipulated the activity of POA^{EP3R} neurons chemogenetically or optogenetically to examine the effect on basal body temperature. Moreover, whether PGE_2 inhibits or excites POA^{EP3R} neurons is unknown, and therefore, the circuit mechanism by which the PGE_2-EP3R signaling in the POA alters the sympathetic outflows through the DMH and rMR to develop fever remains to be determined. It is even controversial whether the POA^{EP3R} neuron group responsible for fever development is GABAergic or glutamatergic (*4*, *17*).

To address these issues, in this study, we investigated the physiological role of POA^{EP3R} neurons in the central circuit mechanisms of thermoregulation and fever, by combining in vivo physiological, chemogenetic, electrophysiological, and neuroanatomical approaches with an antibody to EP3R proteins and a newly developed transgenic rat line that expresses the tetracycline-controlled transactivator (tTA) in EP3R-expressing cells (*Ptger3*-tTA rats). We first examined activation of POA^{EP3R} neurons in response to ambient thermal challenges and then histochemically and physiologically determined the neurotransmitter phenotype of POA^{EP3R} neurons. The impact of chronic heat exposure of animals on the

[1]Department of Integrative Physiology, Nagoya University Graduate School of Medicine, Nagoya 466-8550, Japan. [2]Nagoya University Institute for Advanced Research, Nagoya 464-8601, Japan. [3]Department of Neuroanatomy, Juntendo University Graduate School of Medicine, Tokyo 113-8421, Japan.
*Corresponding author. Email: kazu@med.nagoya-u.ac.jp

transmitter phenotype of POA^{EP3R} neurons was also investigated in relevance to the mechanism of heat tolerance. Last, we examined the effects of chemogenetic manipulations of POA^{EP3R} neuronal activities on sympathetic outflows and thermoregulatory functions.

RESULTS

POA^{EP3R} neurons are activated by ambient heat exposure and project to DMH

To investigate whether POA^{EP3R} neurons are activated in response to ambient thermal challenges, we exposed rats to an environment of 4°C (cold exposure), 24°C (control exposure), or 36°C (heat exposure) for 2 hours and subsequently examined the expression of Fos, a marker for neuronal activation, in POA^{EP3R} neurons by double immunofluorescence histochemistry. Exposure to 4° and 36°C, but not 24°C, activates cold- and warm-sensory afferent neural signaling from the skin to the POA (*6*, *7*). Following control exposure, only a small number of POA^{EP3R} neurons exhibited Fos expression (35 ± 15 in 1280 ± 492 POA^{EP3R} neurons, means ± SEM of four rats; Fig. 1, A and B). Heat exposure remarkably increased Fos-expressing POA^{EP3R} neurons (246 ± 36 in 1525 ± 353 POA^{EP3R} neurons, $n = 4$ rats), but cold exposure did not (36 ± 10 in 1612 ± 299 POA^{EP3R} neurons, $n = 4$ rats; Fig. 1, A and B). These warming-activated POA^{EP3R} neurons were distributed in both MnPO and MPA (Fig. 1C and fig. S1C). These observations indicate that the POA^{EP3R} neuronal group includes a substantial subpopulation of warming-activated neurons but not cooling-activated neurons.

POA^{EP3R} neurons innervate the DMH, which consists of the dorsomedial hypothalamic nucleus and dorsal hypothalamic area (*12*, *13*). To examine whether the warm-responsive POA^{EP3R} neurons project to the DMH, we performed retrograde neural tracing from the DMH. Fluoro-Gold (FG), a retrograde tracer, was bilaterally injected into the hypothalamus to fill most part of the DMH (fig. S1D), and then the rats were exposed to 24° or 36°C for 2 hours. Heat exposure induced Fos expression in more than 60% of FG-labeled POA^{EP3R} neurons (152 ± 17 in 249 ± 42 FG-labeled POA^{EP3R} neurons, $n = 4$ rats), in contrast to few Fos-positive cells following control exposure (12 ± 2 in 236 ± 35 FG-labeled POA^{EP3R} neurons, $n = 3$ rats) (Fig. 1, D and E). These triple-labeled neurons were distributed in both MnPO and MPA (fig. S1E). These results indicate that POA^{EP3R} → DMH transmission is enhanced under conditions in which heat defense is required for thermal homeostasis.

PGE_2 inhibits heat exposure–induced activation of POA^{EP3R} neurons

The EP3R has been shown to be coupled mostly with the inhibitory G protein (G_i) to reduce the intracellular cyclic adenosine monophosphate (cAMP) level in culture cells (*18*). Therefore, we investigated whether a PGE_2 action on POA^{EP3R} neurons inhibits their elevated activity during heat exposure to trigger fever. PGE_2 or saline was injected into the lateral ventricle 10 min before the rats underwent heat exposure (36°C). PGE_2 injection elicited an intense fever, which was characterized by a rapid elevation of body core temperature (T_{core}) by 3.1° ± 0.3°C (means ± SEM, $n = 3$) and maintained throughout heat exposure (Fig. 2A). Rats exposed to heat following saline injection exhibited Fos expression in approximately 30% of POA^{EP3R} neurons (Fig. 2, B and C). This heat exposure–induced Fos expression in POA^{EP3R} neurons was significantly reduced by PGE_2 injection (Fig. 2, B and C). A linear regression analysis based on 1620 to 2366 POA^{EP3R} neuronal cells per rat counted from the whole POA in an unbiased manner revealed a significant negative correlation between Fos expression in POA^{EP3R} neurons and T_{core} at 60 min of heat exposure (Fig. 2D). This analysis predicted that T_{core} would be elevated up to 42.1°C if all POA^{EP3R} neurons were suppressed during heat exposure and that the activation level at which approximately 40% of POA^{EP3R} neurons express Fos would be sufficient for the maintenance of T_{core} around thermoneutral 37°C during heat exposure (Fig. 2D). PGE_2 significantly reduced Fos expression in EP3R-expressing neurons in both MnPO and MPA (Fig. 2E and fig. S2). These results demonstrate that PGE_2 inhibits heat exposure–induced activation of POA^{EP3R} neurons, consistent with the view that the activity of POA^{EP3R} neurons is dynamically altered by warm-sensory inputs to defend T_{core} and by an action of PGE_2 to trigger fever.

POA^{EP3R} neuronal cell bodies predominantly express a glutamatergic marker rather than a GABAergic marker

We next investigated the transmitter phenotype of POA^{EP3R} neurons. In situ hybridization for mRNA of glutamic acid decarboxylase 1 (GAD67; also known as *Gad1*), a marker for GABAergic neurons, or vesicular glutamate transporter 2 (VGLUT2; also known as *Slc17a6*), a marker for glutamatergic neurons, was performed in combination with EP3R immunohistochemistry in the POA. GAD67 and VGLUT2 mRNAs were detected in 22 and 44% of POA^{EP3R} neuronal cell bodies, respectively (GAD67: 352 ± 12 in 1676 ± 198 POA^{EP3R} cell bodies; VGLUT2: 559 ± 55 in 1299 ± 168 POA^{EP3R} cell bodies, means ± SEM, $n = 4$ rats; Fig. 3, A and B). The percentage of POA^{EP3R} cell bodies expressing GAD67 mRNA was lower than that obtained from our previous double-labeling analysis with bright-field microscopy (86%) (*10*), which perhaps made it easier to pick up false-positive cells. Whereas GAD67 and VGLUT2 mRNA expressions were detected in similar percentages of POA^{EP3R} neuronal cell bodies in the rostral half of the POA, the VGLUT2-expressing population was increased in the caudal half of the POA (fig. S3, A and B).

To examine whether POA^{EP3R} neurons expressing GAD67 or VGLUT2 mRNA were activated by heat exposure, we performed triple fluorescence labeling combining EP3R and Fos immunohistochemistry and GAD67 or VGLUT2 in situ hybridization in the POA of rats exposed to 24° or 36°C for 2 hours. Consistent with the aforementioned results, Fos expression following control exposure was detected in only 3 to 5% of POA^{EP3R} cell bodies expressing GAD67 or VGLUT2 mRNA (Fig. 3, C to F). In contrast, heat exposure induced Fos expression in 36 and 61% of POA^{EP3R} cell bodies expressing GAD67 or VGLUT2 mRNA, respectively (72 ± 24 in 193 ± 36 GAD67-expressing POA^{EP3R} cell bodies; 791 ± 63 in 1343 ± 227 VGLUT2-expressing POA^{EP3R} cell bodies, $n = 3$ rats; Fig. 3, C to F). Heat exposure–induced Fos expression in POA^{EP3R} cell bodies expressing either mRNA was observed in both MnPO and MPA (fig. S3, C and D). Therefore, both GAD67 mRNA–expressing and VGLUT2 mRNA–expressing groups of POA^{EP3R} neurons are activated in response to elevation of ambient temperature.

We further performed retrograde tracing to determine whether POA^{EP3R} neurons expressing GAD67 or VGLUT2 mRNA projected to the DMH. Fluorophore-conjugated cholera toxin b subunit

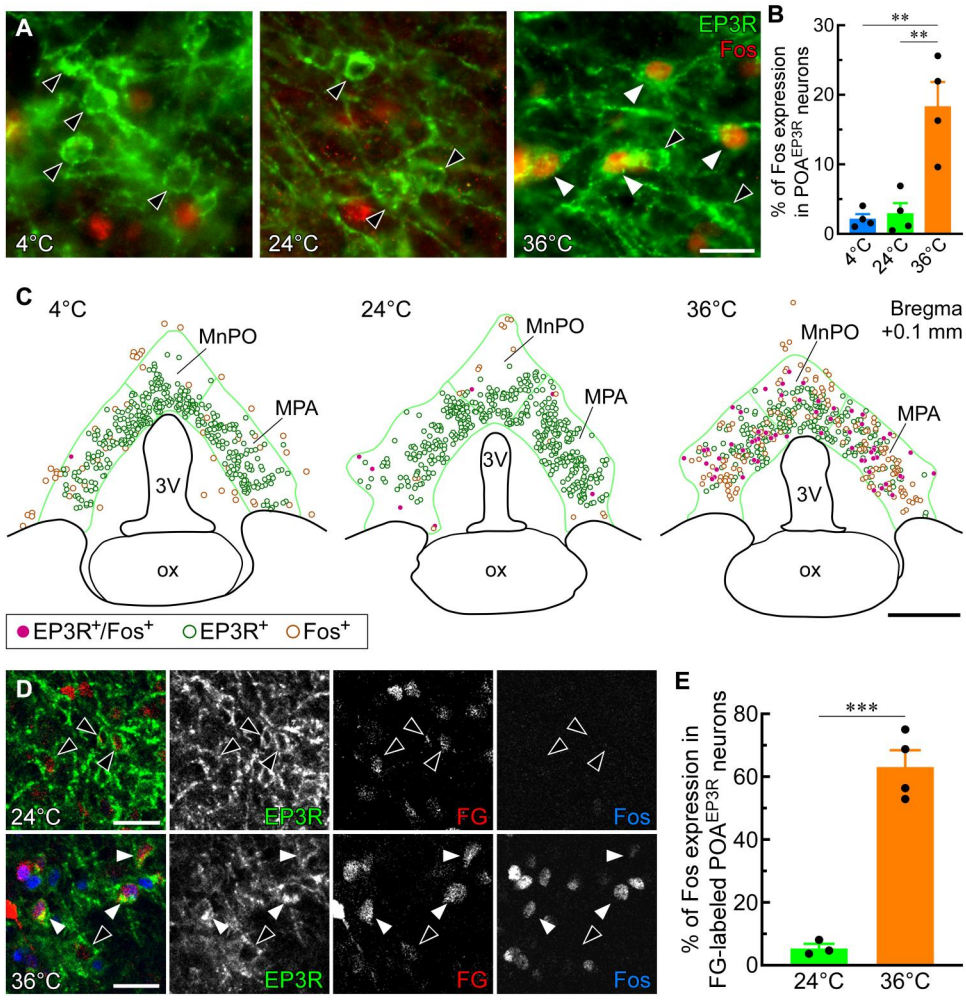

Fig. 1. POA^{EP3R} neurons are activated by ambient heat exposure and project to DMH. (**A**) Double immunofluorescence staining for EP3R and Fos in the POA following a 2-hour exposure of rats to ambient temperature of 4°C (cold), 24°C (control), or 36°C (heat). Solid and hollow arrowheads indicate POA^{EP3R} neuronal cell bodies with and without Fos immunoreactivity, respectively. Scale bar, 20 μm. (**B**) Percentages of Fos expression in POA^{EP3R} neuronal cell bodies (n = 4 per group). $^{**}P < 0.01$ (Bonferroni's post hoc test following ordinary one-way ANOVA: $F_{2,9} = 17.05$, $P < 0.001$). All values are means ± SEM. (**C**) Representative distributions of POA^{EP3R} neurons with and without Fos immunoreactivity following exposure to respective temperature. Scale bar, 0.5 mm. 3V, third ventricle; ox, optic chiasm. Green lines delineate EP3R-immunoreactive areas in the MnPO and MPA, which are anatomically defined in fig. S1A. Distributions of cells with EP3R immunoreactivity and/or Fos immunoreactivity in other POA sections are shown in fig. S1C. (**D**) Pseudo-colored confocal images of Fos immunoreactivity in FG-labeled POA^{EP3R} neuronal cell bodies following a 2-hour exposure of rats to 24° or 36°C ambient temperature. Bilateral FG injections in the DMH for all rats are mapped in fig. S1D. Solid and hollow arrowheads indicate FG-labeled POA^{EP3R} neuronal cell bodies with and without Fos immunoreactivity, respectively. Scale bars, 30 μm. Representative distributions of POA cells labeled with FG, EP3R immunoreactivity, and/or Fos immunoreactivity are shown in fig. S1E. (**E**) Percentages of Fos expression in FG-labeled POA^{EP3R} neuronal cell bodies (n = 3 for 24°C and n = 4 for 36°C). $^{***}P < 0.001$ (unpaired t test; $t_5 = 9.26$). All values are means ± SEM.

(CTb), a retrograde tracer, was unilaterally injected to cover a part of the DMH (fig. S3, E and F). With this size of injection, CTb was detected in 12% of either group of POA^{EP3R} cell bodies with GAD67 or VGLUT2 mRNA (16 ± 2 in 138 ± 30 GAD67-expressing POA^{EP3R} cells; 85 ± 38 in 695 ± 162 VGLUT2-expressing POA^{EP3R} cells, n = 3 rats; Fig. 3, G and H). CTb-labeled POA^{EP3R} neurons consisted of 20% of GAD67-expressing cells and 81% of VGLUT2-expressing cells (fig. S3G). These results indicate that both GAD67 mRNA– and VGLUT2 mRNA–expressing groups of POA^{EP3R} neurons provide axonal projections to the DMH.

POA^{EP3R} → DMH axon terminals predominantly contain a GABAergic marker rather than a glutamatergic marker

To more directly determine the neurotransmitters used for POA^{EP3R} → DMH transmission, we sought to perform anterograde tract tracing specifically from POA^{EP3R} neurons. For this purpose, we generated a *Ptger3*-tTA transgenic rat line in which tTA was expressed under the promoter of the *Ptger3* (EP3R) gene (fig. S4). Injection into the POA of *Ptger3*-tTA rats with the adeno-associated virus (AAV) vector, AAV-TRE-palGFP, to express palGFP, a membrane-targeted form of green fluorescent protein (GFP) (*19*), under the control of the tetracycline response element (TRE) resulted in highly selective labeling of POA^{EP3R} neurons with palGFP: Distribution of palGFP-labeled cells well overlapped with that of POA^{EP3R}

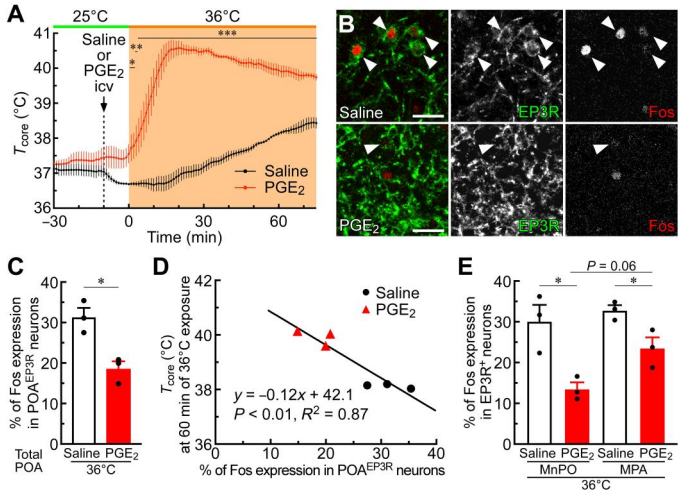

Fig. 2. PGE_2 inhibits heat exposure–induced activation of POA^{EP3R} neurons. (**A**) Changes in T_{core} of rats during exposure to 36°C ambient temperature following intracerebroventricular (icv) injection of saline or PGE_2 ($n = 3$ per group) were analyzed by repeated-measures two-way ANOVA (injectant: $F_{1,4} = 207.1$, $P < 0.001$; time: $F_{105,420} = 42.74$, $P < 0.001$; interaction: $F_{105,420} = 22.83$, $P < 0.001$) followed by Bonferroni's post hoc test (*$P < 0.05$, **$P < 0.01$, and ***$P < 0.001$; horizontal bars with asterisks indicate time points with significant difference). All values are means ± SEM. (**B**) Confocal images of Fos immunoreactivity in POA^{EP3R} neuronal cell bodies following intracerebroventricular injection of saline or PGE_2 and exposure to 36°C ambient temperature. Heat exposure increased Fos expression in POA^{EP3R} neurons (arrowheads; top), which was reduced by PGE_2 injection (bottom). Scale bars, 30 μm. Representative distributions of POA cells with EP3R immunoreactivity and/or Fos immunoreactivity are shown in fig. S2. (**C**) Percentages of Fos expression in POA^{EP3R} neurons following heat exposure after saline or PGE_2 injection ($n = 3$ per group). *$P < 0.05$ (unpaired t test; $t_4 = 4.34$). All values are means ± SEM. (**D**) Relationship between the percentage of Fos expression in POA^{EP3R} neurons and T_{core} of the rats at 60 min of heat exposure. Data from the saline-injected and PGE_2-injected groups were subjected to linear regression analysis (Pearson's correlation test). (**E**) Percentages of Fos expression in EP3R-immunoreactive cell bodies in the MnPO and MPA following heat exposure after saline or PGE_2 injection ($n = 3$ per group). *$P < 0.05$ (unpaired t tests; saline versus PGE_2 in MnPO: $t_4 = 3.78$; saline versus PGE_2 in MPA: $t_4 = 3.12$; paired t tests; MnPO-saline versus MPA-saline: $t_2 = 0.67$; MnPO-PGE_2 versus MPA-PGE_2: $t_2 = 3.83$). All values are means ± SEM.

neurons, and 97% of palGFP-labeled neurons were immunopositive for EP3R (Fig. 4, A and B).

The expression of palGFP clearly visualized the axonal morphology of POA^{EP3R} neurons to their terminals, and palGFP-labeled axons were widely observed in the hypothalamus, thalamus, amygdala, midbrain, pons, and medulla oblongata. Dense distribution of palGFP-labeled axon fibers and terminals was observed in the DMH (Fig. 4C). Other brain regions in which palGFP-labeled axon fibers and terminals were distributed include the paraventricular hypothalamic nucleus, hypothalamic arcuate nucleus, perifornical area, medial tuberal nucleus, peduncular part of the lateral hypothalamus, anterior parts of the mediodorsal and paraventricular thalamic nuclei, lateral habenular nucleus, basolateral amygdaloid nucleus, ventral subiculum, lateral and ventrolateral periaqueductal gray, lateral parabrachial nucleus, raphe magnus nucleus, rostral raphe pallidus nucleus, and a transition area between the caudal raphe pallidus and raphe obscurus nuclei (Fig. 4C and fig. S5).

The palGFP-labeled axons in the DMH often formed basket-like structures with axonal boutons (Fig. 4D), putative synaptic contacts. Therefore, we performed confocal laser scanning microscopy to detect vesicular transporters for the fast transmitters, GABA and glutamate, in palGFP-labeled DMH-projecting axons of POA^{EP3R} neurons. Unexpectedly, palGFP-labeled axons in the DMH contained abundant puncta immunoreactive for vesicular GABA transporter (VGAT), a marker for GABAergic presynaptic terminals, whereas VGLUT2-immunoreactive puncta, indicating glutamatergic terminals, were only occasionally found in these axons (Fig. 4, E and F, and fig. S6A; for quantification data, see below and Fig. 4G). Some of the VGLUT2-immunoreactive puncta also exhibited VGAT immunoreactivity (fig. S6B).

Most VGAT-immunoreactive puncta in palGFP-labeled axons in the DMH were immunoreactive for synaptophysin (fig. S6C), confirming that these puncta constitute presynaptic structures. In addition, immunoreactivity for GAD67, a GABA-synthesizing enzyme, was colocalized with or in close proximity to many VGAT-immunoreactive puncta in palGFP-labeled axons in the DMH (fig. S6D), indicating the capability of local GABA production in those VGAT-containing presynaptic structures. Validating the specificity of the anti-VGAT guinea pig antibody used for the histochemical analyses, VGAT-immunoreactive profiles visualized by this antibody in the DMH were colabeled well with mouse and rabbit antibodies raised against different epitopes on the VGAT protein (fig. S6E). To validate our VGLUT2 immunohistochemistry, we tested whether the anti-VGLUT2 antibody used can visualize the axon terminals of thalamocortical neurons, which mostly express VGLUT2 (*20*). Injection of AAV-TRE-palGFP into the anterior midline thalamus of *Ptger3*-tTA rats transduced many neurons in the anterior part of the paraventricular thalamic nucleus and central medial thalamic nucleus with palGFP (fig. S7A), consistent with intense EP3R expression in these nuclei (*15*). Their palGFP-labeled axons were densely distributed in the area 2 of the cingulate cortex and contained many VGLUT2-immunoreactive puncta (fig. S7B) but few VGAT-immunoreactive puncta (83 and 4% of 1725 immunoreactive puncta counted in palGFP-labeled axons in the area 2 of the cingulate cortex, respectively). Some double immunoreactive puncta (13%) were also observed. These data validate our immunohistochemical analyses of transporter localization in POA^{EP3R} → DMH axon terminals.

The DMH contains glutamatergic neurons that transmit sympathoexcitatory signals to sympathetic premotor neurons in the rMR to drive thermogenic responses for cold defense and fever (*11*, *12*, *21*–*25*). Retrograde labeling with FG injected into the rMR visualized a dense cluster of rMR-projecting neurons in the DMH (fig. S7, C and D) (*12*, *26*). These FG-labeled cell bodies were often closely associated with palGFP-labeled axon swellings (168 ± 20 swellings in contact were found, means ± SEM of four rats), suggestive of synaptic contacts, and a substantial number (60 ± 6) of these axon swellings contained VGAT (Fig. 4H), but few (3 ± 2) were VGLUT2 positive. In addition, 3 ± 2 swellings in contact were immunoreactive for both VGAT and VGLUT2. These observations support the view that POA^{EP3R} → DMH projection neurons regulate DMH → rMR sympathoexcitatory neurons via GABAergic synaptic inputs rather than glutamatergic inputs.

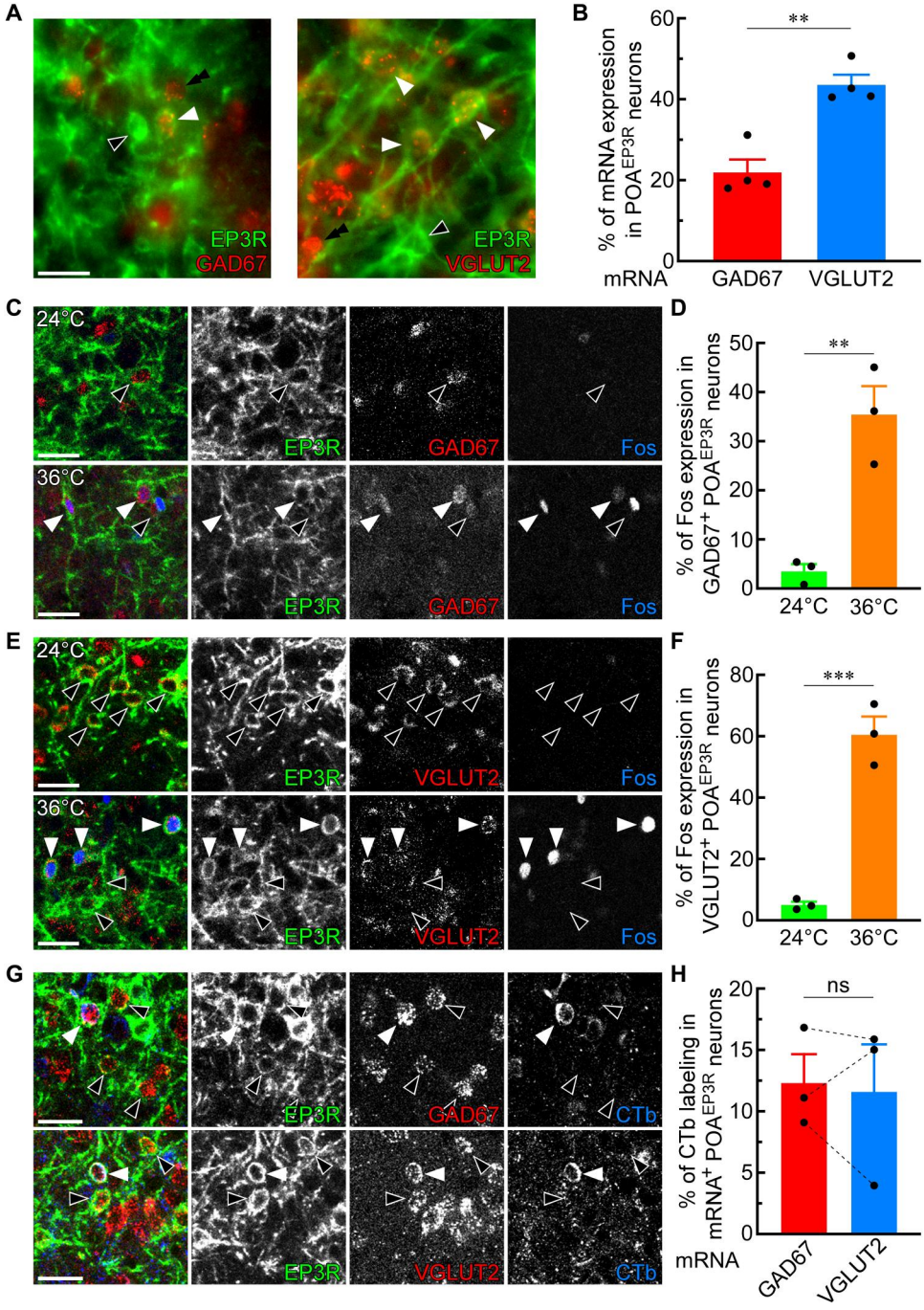

Fig. 3. POA^{EP3R} neuronal cell bodies predominantly express a glutamatergic marker rather than a GABAergic marker. (**A**) Double fluorescence labeling with EP3R immunoreactivity and GAD67 or VGLUT2 mRNA hybridization signals in POA neurons. Solid and hollow arrowheads indicate POA^{EP3R} neuronal cell bodies with and without mRNA signals, respectively. Double arrowheads indicate mRNA signals in EP3R-immunonegative cells. Scale bar, 20 μm. For distribution, see fig. S3 (A and B). (**B**) Percentages of GAD67 and VGLUT2 mRNA expression in POA^{EP3R} neuronal cell bodies (n = 4 per group). $^{**}P < 0.01$ (unpaired t test; $t_6 = 5.56$). All values are means ± SEM. (**C** to **F**) Confocal images of Fos immunoreactivity in GAD67 mRNA–expressing (C) or VGLUT2 mRNA–expressing (E) POA^{EP3R} neuronal cell bodies following 24° or 36°C exposure of rats for 2 hours. Solid and hollow arrowheads indicate mRNA-expressing POA^{EP3R} neuronal cell bodies with and without Fos immunoreactivity, respectively. Scale bars, 30 μm. Exposure to 36°C increased Fos expression in POA^{EP3R} neurons expressing GAD67 (D) and VGLUT2 (F) mRNA (n = 3 per group). $^{**}P < 0.01$ and $^{***}P < 0.001$ [unpaired t tests; $t_4 = 5.43$ (D) and $t_4 = 9.50$ (F)]. All values are means ± SEM. For distribution, see fig. S3 (C and D). (**G** and **H**) Pseudo-colored confocal images of GAD67 (top) (G) or VGLUT2 (bottom) (G) mRNA–expressing POA^{EP3R} neuronal cell bodies with immunoreactivity for CTb derived from the DMH. Solid and hollow arrowheads indicate mRNA-expressing POA^{EP3R} neuronal cell bodies with and without CTb immunoreactivity, respectively. Scale bars, 30 μm. Percentages of CTb labeling were comparable between GAD67 mRNA–expressing and VGLUT2 mRNA–expressing POA^{EP3R} neurons (H) (n = 3). ns, not significant (paired t test; $t_2 = 0.27$). All values are means ± SEM. CTb injection sites for all the rats are shown in fig. S3 (E and F). See also fig. S3G.

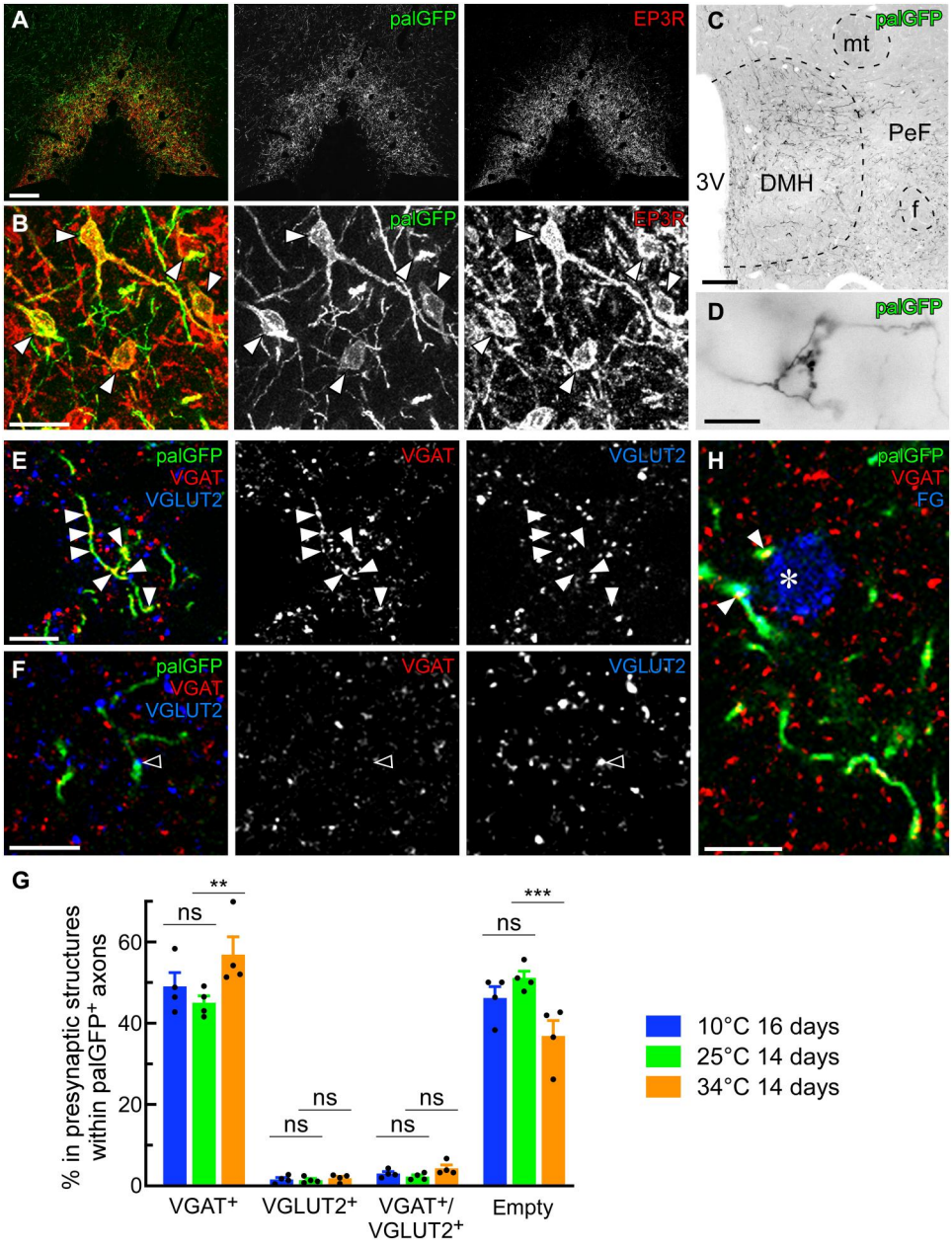

Fig. 4. POA^{EP3R}→ DMH axon terminals predominantly contain a GABAergic marker rather than a glutamatergic marker. (**A** and **B**) Selective transduction of POA^{EP3R} neurons with palGFP by injecting AAV-TRE-palGFP into the POA of *Ptger3*-tTA rats (A). Magnified confocal images (B) show palGFP-expressing POA^{EP3R} neurons (arrows). Scale bars, 0.2 mm (A) and 30 μm (B). (**C** and **D**) The composite fluorescence image (C) shows the distribution of POA^{EP3R} neuron–derived, palGFP-immunoreactive axons in the DMH and perifornical area (PeF). The magnified image (D) shows basket-like structures with axonal boutons in the DMH. Scale bars, 0.2 mm (C) and 10 μm (D). f, fornix; mt, mammillothalamic tract. For distribution in other brain regions, see fig. S5. (**E** and **F**) Confocal images of palGFP-labeled (POA^{EP3R} neuron–derived) axons with VGAT-immunoreactive (solid arrowheads) (E) and VGLUT2-immunoreactive (hollow arrowhead) (F) puncta in the DMH. Scale bars, 10 μm. Other confocal images are presented in fig. S6. (**G**) Percentages of VGAT-immunoreactive puncta (VGAT$^+$), VGLUT2-immunoreactive puncta (VGLUT2$^+$), double immunoreactive puncta (VGAT$^+$/VGLUT2$^+$), and double immunonegative axon swellings (Empty) in total of the axonal presynaptic structures in palGFP-labeled axons in the DMH of *Ptger3*-tTA rats exposed to 10°, 25°, or 34°C for 14 to 16 days (n = 4 rats per group). Data were analyzed by repeated-measures two-way ANOVA (transmitter marker: $F_{3,27} = 309.8$, $P < 0.001$; temperature: $F_{2,9} = 0.43$, $P = 0.66$; interaction: $F_{6,27} = 4.52$, $P < 0.01$) followed by Bonferroni's post hoc test (**$P < 0.01$ and ***$P < 0.001$). All values are means ± SEM. (**H**) A pseudo-colored confocal image of VGAT-immunoreactive, palGFP-labeled (POA^{EP3R} neuron–derived) axon swellings (arrowheads) that are apposed to a DMH neuronal cell body (asterisk) retrogradely labeled with FG from the rMR. Scale bar, 10 μm. A representative retrograde labeling of DMH → rMR projection neurons with FG is shown in fig. S7 (C and D).

Chronic heat exposure increases GABAergic POA^{EP3R} → DMH axon terminals

Because POA^{EP3R} neurons are responsive to ambient thermal challenges (Fig. 1), we investigated whether the localization of the vesicular transporters in POA^{EP3R} → DMH axon terminals was altered by chronic exposure to extreme temperatures. *Ptger3*-tTA rats injected with AAV-TRE-palGFP into the POA were exposed to 10°C (cold exposure), 25°C (control exposure), or 34°C (heat exposure) for 14 to 16 days, and we subsequently quantified VGAT- and VGLUT2-immunopositive puncta in palGFP-labeled axons in the DMH as presynaptic sites that release GABA and glutamate, respectively. Because there were also a substantial number of palGFP-labeled axon swellings that contained neither VGAT- nor VGLUT2-immunoreactive profile, we also quantified these "empty" swellings that were more than 1.5 times thicker than the adjacent axon shaft; most swellings that exceeded this threshold thickness were found to contain synaptophysin in our preliminary analyses.

Among 6123 ± 1152 (means ± SEM) palGFP-labeled axonal presynaptic structures (i.e., total of VGAT- and/or VGLUT2-immunoreactive puncta and empty swellings) counted bilaterally in the DMH of rats (n = 4) exposed to 25°C, 45% were VGAT-immunoreactive puncta, and 51% were empty swellings (Fig. 4G). In contrast, only 1% were VGLUT2-immunoreactive puncta, and 2% were double immunoreactive puncta (Fig. 4G). Following chronic heat exposure, the population of VGAT-immunoreactive puncta was significantly increased to 57%, and empty swellings were reduced to 37%, whereas the VGLUT2-immunoreactive populations were not affected (8065 ± 2432 palGFP-labeled axonal presynaptic structures counted in the DMH; n = 4 rats; Fig. 4G). Chronic cold exposure did not alter any of the populations (6462 ± 2284 palGFP-labeled axonal presynaptic structures counted in the DMH; n = 4 rats), compared to control exposure (Fig. 4G). These data suggest a mechanism of heat adaptation, in which POA^{EP3R} neurons increase their GABAergic synapses onto sympathoexcitatory DMH neurons under chronic heat exposure, so that they can more efficiently inhibit thermogenic and other sympathetic outflows to tolerate heat.

POA^{EP3R} → DMH axon terminals predominantly release GABA

To physiologically determine the transmitter released from POA^{EP3R} → DMH axon terminals, we performed slice patch-clamp recordings from DMH neurons combined with optogenetic stimulation of POA^{EP3R} → DMH axon terminals (Fig. 5A). ChIEF, an engineered channelrhodopsin variant used for optogenetic stimulation of axon terminals (*25*), was selectively expressed in POA^{EP3R} neurons by AAV injection into the POA of *Ptger3*-tTA rats [87% of enhanced yellow fluorescent protein (EYFP)–expressing neurons were EP3R immunoreactive; Fig. 5B]. Expressed ChIEF-EYFP proteins were distributed in POA^{EP3R} → DMH axon fibers (Fig. 5C). In DMH tissue slices, we found eight neuronal cells in which blue light pulses faithfully evoked postsynaptic currents in the presence of tetrodotoxin (TTX) and 4-aminopyridine (4-AP), blockers of voltage-gated Na^+ and K^+ channels, respectively, indicating that the currents were monosynaptically evoked. In our recording condition with a CsCl-based internal solution and the membrane potential held at −50 mV, the optically evoked postsynaptic currents (oPSCs) were inward currents that were potentially a mixture of glutamatergic and GABAergic postsynaptic currents (Fig. 5D). In seven of the eight DMH neurons, the oPSCs were scarcely affected by a mixture of 6-cyano-7-nitroquinoxaline-2,3-dione (CNQX) and D-(−)-2-amino-5-phosphonopentanoic acid (AP5), which are AMPA and *N*-methyl-D-aspartate (NMDA) glutamate receptor antagonists, respectively; however, subsequent application of bicuculline, a GABA type A receptor antagonist, completely eliminated oPSCs (Fig. 5, D and E). The remaining one neuron exhibited an oPSC that was eliminated by CNQX and AP5 (Fig. 5F). These results demonstrate that POA^{EP3R} neuron–derived axons predominantly form GABAergic synapses onto DMH neurons.

Chemogenetic manipulations of POA^{EP3R} neurons bidirectionally alter body temperature by eliciting effector responses

We examined the effects of selective in vivo inhibition and stimulation of POA^{EP3R} neurons on thermoregulation at room temperature by using chemogenetic techniques with hM4Di and hM3Dq, G_i- and G_q-coupled designer receptors exclusively activated by designer drug (DREADDs) (*27*), respectively (Fig. 6). To inhibit POA^{EP3R} neurons, we used hM4Di^{nrxn}, an axon-targeted variant of hM4Di conjugated with an intracellular domain of neurexin 1α (*28*). Activation of the inhibitory DREADD hM4Di^{nrxn} at presynaptic structures suppresses synaptic release probability (*28*). POA^{EP3R} neurons were selectively transduced with hM4Di^{nrxn} by injecting AAV-TRE-mCherry-T2A-hM4Di^{nrxn} into the POA of *Ptger3*-tTA rats (95% of mCherry-expressing neurons were EP3R immunoreactive; Fig. 6, A and B). In these rats, an injection into the lateral ventricle with DREADD Agonist 21 [11-(1-piperazinyl)-5*H*-dibenzo[*b*,*e*][1,4]diazepine dihydrochloride (C21)], a selective actuator for the DREADDs (*29*), increased T_{core} and BAT temperature (T_{BAT}) by 2.5° ± 0.2°C and 2.6° ± 0.2°C (means ± SEM, n = 4), respectively, whereas saline injection had no effect on these thermal variables (Fig. 6D). In the initial phase of the temperature rise, the elevation of T_{BAT} led that of T_{core} (Fig. 6G), suggesting that BAT was a source of heat for the development of the hyperthermia. On the other hand, activity levels of the rats, which could also contribute to heat production, were not obviously affected by C21 (Fig. 6D). The hyperthermic state was maintained for approximately 8 hours and returned to baseline by 9 hours after C21 injection (Fig. 6D).

For stimulation of POA^{EP3R} neurons, AAV-TRE-hM3Dq-mCherry was injected into the POA of *Ptger3*-tTA rats to selectively express hM3Dq in POA^{EP3R} neurons (83% of mCherry-expressing neurons exhibited EP3R immunoreactivity; Fig. 6, A and C). In contrast to the hyperthermia induced by inhibition of POA^{EP3R} neurons, injection of C21 into the lateral ventricle of *Ptger3*-tTA rats with POA^{EP3R} neurons expressing hM3Dq induced hypothermia: T_{core} and T_{BAT} were reduced by 1.9° ± 0.9°C and 2.2° ± 0.9°C (n = 5), respectively (Fig. 6E). Thermography during the drop in T_{core} revealed marked increases in tail skin temperature and whole-body surface temperature (Fig. 6, H and I), indicating the induction of an active heat loss response via increased skin blood flow. The hypothermic T_{core} (below 36.0°C) was maintained until 7 to 9 hours after C21 injection (Fig. 6E). Saline injection induced no obvious change in T_{core}, T_{BAT}, or tail skin temperature (Fig. 6, E and I). C21 did not affect the activity levels of the rats (Fig. 6E). In control *Ptger3*-tTA rats, which expressed palGFP in POA^{EP3R} neurons, C21 had no effect on T_{core}, T_{BAT}, or activity (Fig. 6F). These in vivo physiological data demonstrate that changes in the

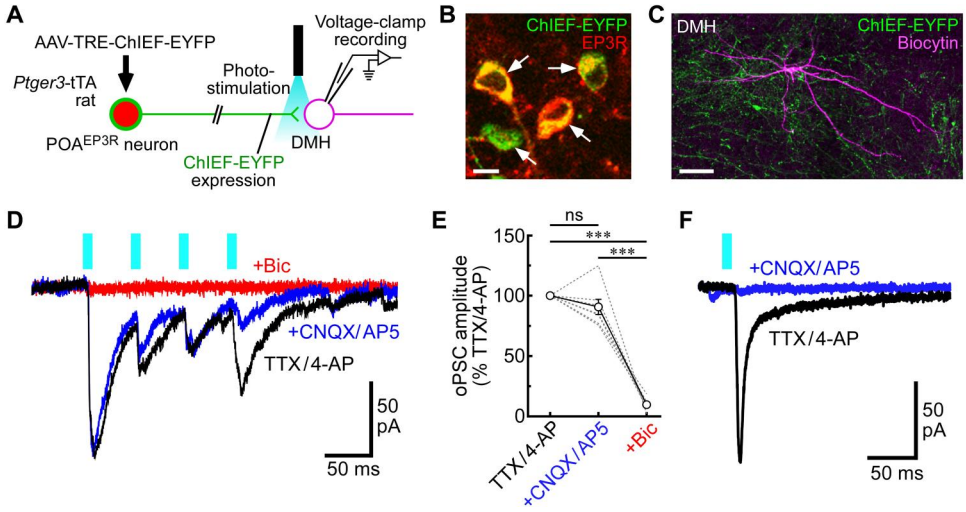

Fig. 5. POA^{EP3R}→ DMH axon terminals predominantly form GABAergic synapses onto DMH neurons. (**A**) Slice patch-clamp (voltage-clamp) recording from single DMH neurons in combination with optogenetic photostimulation of POA^{EP3R} → DMH axon terminals. (**B**) Selective transduction of POA^{EP3R} neurons with ChIEF-EYFP (arrows) by injecting AAV-TRE-ChIEF-EYFP into the POA of *Ptger3*-tTA rats. Scale bar, 10 μm. (**C**) A recorded DMH neuron labeled with biocytin (pseudo-colored) was associated with many ChIEF-EYFP–bearing axon fibers derived from POA^{EP3R} neurons. Scale bar, 100 μm. (**D**) oPSCs recorded from the neuron shown in (C). Pulsed illumination in the presence of TTX/4-AP faithfully evoked oPSCs, which were scarcely affected by an addition of CNQX/AP5. However, a subsequent addition of bicuculline (Bic) eliminated oPSCs. Seven of eight DMH neurons in which we could record oPSCs exhibited predominantly GABAergic postsynaptic currents, as did this neuron. Each trace shows the average of 10 stimulation trials. (**E**) oPSC amplitude after each drug treatment in the seven DMH neurons that exhibited predominantly GABAergic postsynaptic currents. oPSCs evoked by the first photostimulation were averaged through 10 trains for each neuron. Data were analyzed by repeated-measures one-way ANOVA ($F_{2,12}$ = 138, P < 0.001) followed by Bonferroni's post hoc test (***P < 0.001). All values are means ± SEM. (**F**) One remaining DMH neuron that exhibited an oPSC eliminated by CNQX/AP5.

activity of POA^{EP3R} neurons alter T_{core} bidirectionally via altering the regulations of BAT thermogenesis and cutaneous vasoconstrictors.

POA^{EP3R} → DMH transmission tonically inhibits sympathetic outflow to BAT

The present anatomical and physiological results suggest that POA^{EP3R} → DMH projection neurons provide tonic GABAergic inhibitory signals to regulate the DMH → rMR sympathoexcitatory pathway, and a reduction of the GABAergic signal tones results in disinhibition of the sympathoexcitatory pathway, leading to BAT thermogenesis and hyperthermia. Consistent with this possibility, local inhibition of POA^{EP3R} → DMH axon terminals by bilateral nanoinjections of C21 into the DMH of *Ptger3*-tTA rats that expressed hM4Di^{nrxn} in POA^{EP3R} neurons elicited robust increases in BAT sympathetic nerve activity (SNA), T_{BAT}, expired CO_2 (an index of systemic metabolism), and heart rate (HR) in an anesthetized preparation (Fig. 7, A and B, and Table 1). This result indicates that withdrawal of the tonic GABAergic inhibition of sympathoexcitatory DMH neurons by POA^{EP3R} neurons is sufficient to induce BAT thermogenesis and tachycardia.

On the other hand, there is also POA → DMH glutamatergic transmission that could provide an excitation to sympathoexcitatory DMH neurons after withdrawal of the GABAergic inhibition from POA^{EP3R} neurons (*30*–*32*). The balance between GABAergic and glutamatergic inputs from the POA to the DMH is considered important for proper control of the DMH → rMR neurons that drive thermogenic sympathetic outflow (*3*, *4*). To examine whether POA^{EP3R} → DMH neurons contribute to this excitatory/inhibitory (E/I) balance control of sympathetic efferent signaling, we tested the effect of local inhibition of POA^{EP3R} → DMH axon terminals on BAT thermogenesis and cardiovascular responses evoked by a glutamatergic excitation in the DMH (Fig. 7). A unilateral nanoinjection of NMDA, an ionotropic glutamate receptor agonist, into the DMH consistently elicited increases in BAT SNA, T_{BAT}, expired CO_2, HR, and mean arterial pressure in either *Ptger3*-tTA rats that expressed hM4Di^{nrxn} in POA^{EP3R} neurons or control *Ptger3*-tTA rats that expressed palGFP in POA^{EP3R} neurons (Fig. 7, C to E). A unilateral nanoinjection of C21 into the DMH by itself did not elicit any response but did potentiate the BAT thermogenic, metabolic (expired CO_2), and pressor responses evoked by a subsequent NMDA nanoinjection at the same DMH site in hM4Di^{nrxn}-expressing rats (Fig. 7, D and E). However, this potentiation did not occur in control rats (Fig. 7, C and E). These results support the view that POA^{EP3R} → DMH transmission provides tonic inhibitory signals to control sympathoexcitatory DMH neurons, and reduction of this tonic inhibition results in an E/I balance shift to enhance the excitability of sympathoexcitatory DMH neurons to drive BAT thermogenesis and cardiovascular responses.

DISCUSSION

The POA has been considered as a thermoregulatory center and a febrile center (*1*, *33*). The present study demonstrates that POA^{EP3R} neurons, a target of PGE_2 for its pyrogenic action, play a pivotal role in the preoptic efferent control of central sympathetic outflow for basal thermoregulation. Heat exposure of rats increased Fos expression in POA^{EP3R} neurons, and chemogenetic stimulation of POA^{EP3R} neurons elicited hypothermia at room temperature via a remarkable increase in skin blood flow, an active heat loss response

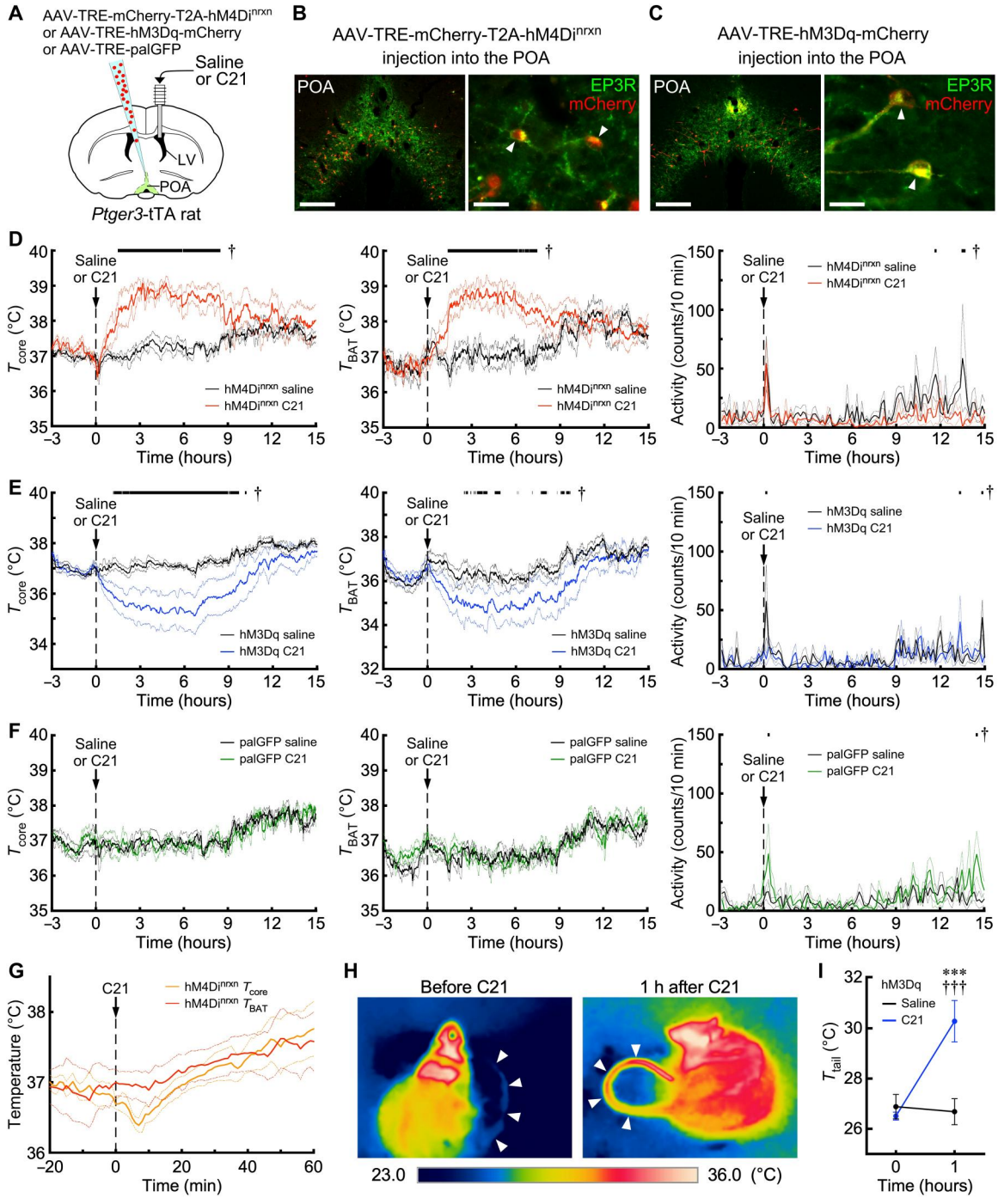

Fig. 6. Chemogenetic manipulations of POA^{EP3R} neurons bidirectionally alter body temperature by eliciting effector responses. (**A**) The injection scheme for in vivo chemogenetic experiments. LV, lateral ventricle. (**B** and **C**) Representative examples showing selective transduction of POA^{EP3R} neurons with mCherry-T2A-hM4Di^{nrxn} (B) and hM3Dq-mCherry (C) in *Ptger3*-tTA rats. Arrowheads indicate POA^{EP3R} neuronal cell bodies labeled with mCherry. Scale bars, 0.3 mm (left) and 30 μm (right). (**D** to **G**) Time-course changes in T_{core}, T_{BAT}, and activity following intracerebroventricular injection of saline or C21 in *Ptger3*-tTA rats with POA^{EP3R} neurons transduced with mCherry-T2A-hM4Di^{nrxn} (n = 4 per group) (D), hM3Dq-mCherry (n = 5 per group) (E), or palGFP (n = 4 per group) (F). The injection was made at 10 a.m., and the dark period started at 9 hours after the injection. Data were analyzed by repeated-measures two-way ANOVA (see table S1) followed by Bonferroni's post hoc test (horizontal bars with † indicate time points with difference at a statistically significant level of $P < 0.05$). The graph in (G) compares the changes in T_{core} and T_{BAT} for 60 min after C21 injection in *Ptger3*-tTA rats with POA^{EP3R} neurons transduced with mCherry-T2A-hM4Di^{nrxn} (n = 4 per group). All values are means ± SEM. (**H** and **I**) Thermographic measurements of the tail skin (arrowheads) in *Ptger3*-tTA rats with POA^{EP3R} neurons transduced with hM3Dq-mCherry (n = 4) before and 1 hour after C21 injection. The difference in tail skin temperature (T_{tail}) at each time point was analyzed by repeated-measures two-way ANOVA (injectant: $F_{1,3}$ = 17.17, P = 0.026; time: $F_{1,3}$ = 5.69, P = 0.097; interaction: $F_{1,3}$ = 405.6, $P < 0.001$) followed by Bonferroni's post hoc test. ***$P < 0.001$ (versus saline) and †††$P < 0.001$ (versus time 0). All values are means ± SEM.

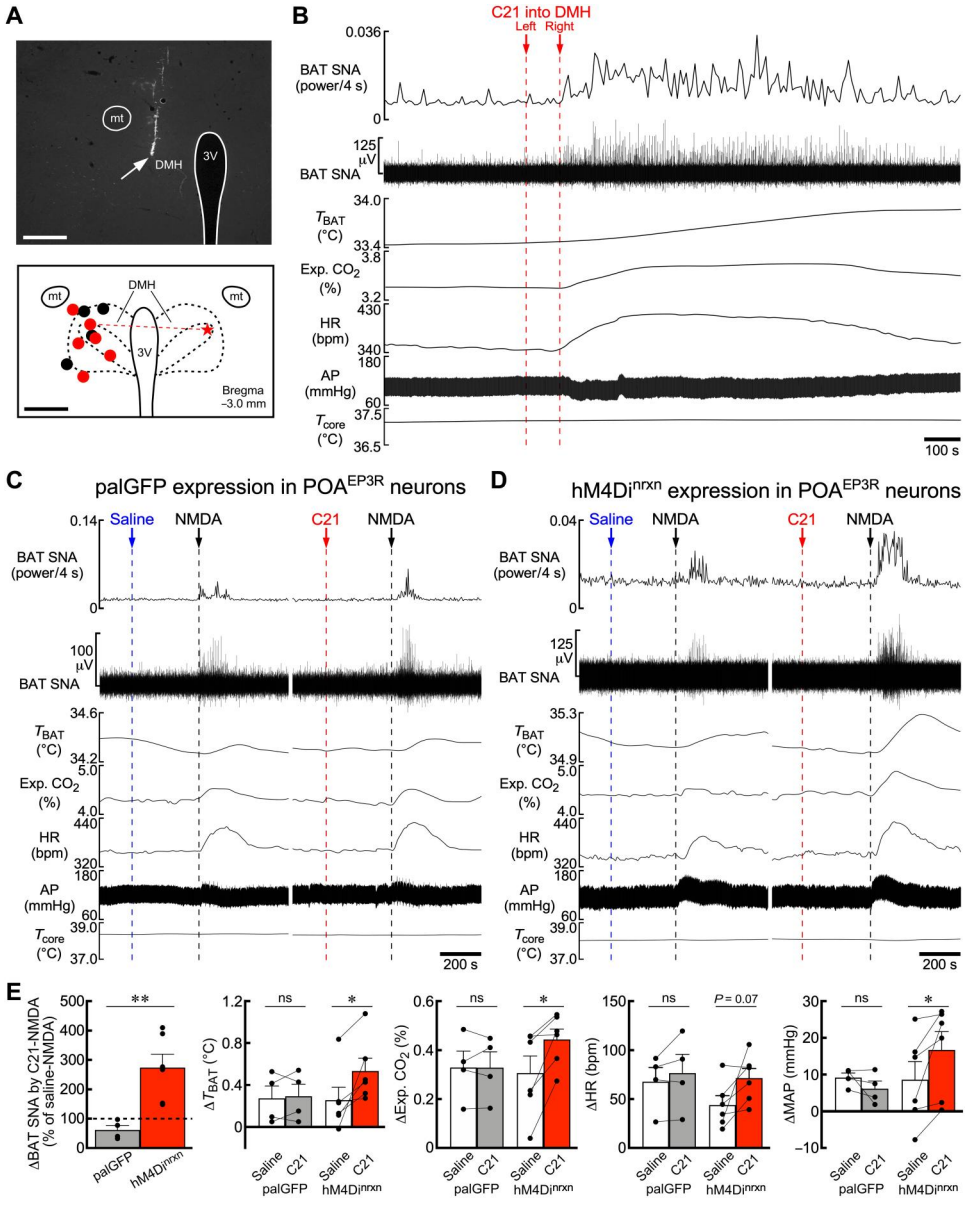

Fig. 7. POA^{EP3R}→ DMH transmission tonically inhibits sympathetic outflow to BAT. (**A**) A representative nanoinjection (arrow) (top) in the DMH and a map (bottom) showing all unilateral injection sites in the DMH of *Ptger3*-tTA rats with POA^{EP3R} neurons transduced with palGFP (black circles) or mCherry-T2A-hM4Di^{nrxn} (red circles) for (E) and bilateral C21 injections in (B) (symbols tied with a dashed line). Scale bars, 0.5 mm. (**B**) Example of increases in BAT thermogenesis (BAT SNA and T_{BAT}), expired (Exp.) CO_2, and HR evoked by bilateral nanoinjections of C21 into the DMH of a *Ptger3*-tTA rat with POA^{EP3R} neurons transduced with mCherry-T2A-hM4Di^{nrxn}. AP, arterial pressure; bpm, beats per minute. For group data, see Table 1. (**C** and **D**) Effects of unilateral nanoinjection of saline or C21 into the DMH of *Ptger3*-tTA rats with POA^{EP3R} neurons transduced with palGFP (C) or mCherry-T2A-hM4Di^{nrxn} (D) on increases in physiological variables evoked by NMDA injection at the same DMH site. (**E**) Group data showing NMDA-induced changes in physiological variables following saline or C21 injection into the DMH of *Ptger3*-tTA rats with POA^{EP3R} neurons transduced with palGFP ($n = 4$) or mCherry-T2A-hM4Di^{nrxn} ($n = 6$). NMDA-evoked increases in BAT SNA following C21 injection are expressed as % of those following saline injection and compared between the palGFP and mCherry-T2A-hM4Di^{nrxn} groups by an unpaired *t* test ($t_8 = 3.65$). NMDA-induced changes in T_{BAT}, Exp. CO_2, HR, and mean arterial pressure (MAP) following saline and C21 injection were compared by paired *t* tests (T_{BAT}: palGFP, $t_3 = 0.37$; hM4Di^{nrxn}, $t_5 = 3.15$; Exp. CO_2: palGFP, $t_3 = 0.02$; hM4Di^{nrxn}, $t_5 = 3.53$; HR: palGFP, $t_3 = 1.30$; hM4Di^{nrxn}, $t_5 = 2.34$; MAP: palGFP, $t_3 = 1.47$; hM4Di^{nrxn}, $t_5 = 2.70$). *$P < 0.05$ and **$P < 0.01$. All values are means ± SEM. For the procedure of data analyses, see Materials and Methods.

Table 1. Bilateral chemogenetic inhibition of POA^{EP3R}→ DMH axon terminals increases BAT thermogenesis, whole-body metabolism, and HR. BAT SNA, T_{BAT}, expired (Exp.) CO_2, HR, and mean arterial pressure (MAP) were measured before and after bilateral nanoinjections of C21 into the DMH of *Ptger3*-tTA rats ($n = 6$) with POA^{EP3R} neurons transduced with mCherry-T2A-hM4Di^{nrxn} (see also Fig. 7B). Pre- and postinjection values (means ± SEM) are compared by paired *t* tests (**$P < 0.01$ and ***$P < 0.001$). For the procedure of data analyses, see Materials and Methods.

	Preinjection	Postinjection	*t*
BAT SNA (% baseline)	100	289.6 ± 36.1**	$t_5 = 5.26$
T_{BAT} (°C)	34.4 ± 0.3	35.0 ± 0.3**	$t_5 = 4.80$
Exp. CO_2 (%)	4.4 ± 0.2	4.8 ± 0.2***	$t_5 = 7.00$
HR (bpm)	351.6 ± 15.9	410.7 ± 16.1**	$t_5 = 5.27$
MAP (mmHg)	114.2 ± 6.2	117.9 ± 5.6	$t_5 = 1.67$

mediated by sympathoinhibition. On the other hand, chemogenetic inhibition of POA^{EP3R} neurons elicited hyperthermia via an increase in BAT thermogenesis, mimicking fever and cold defense. Therefore, the POA^{EP3R} neuron group bidirectionally regulates T_{core} by controlling both production and dissipation of heat. Our histochemical and electrophysiological analyses further showed that POA^{EP3R} neurons provide predominantly GABAergic innervation to sympathoexcitatory DMH neurons whose activation increases T_{core} via excitation of sympathetic premotor neurons in the rMR. The POA has been considered to provide descending tonic inhibitory signaling to regulate thermoregulatory sympathetic outflow, because disruption of this inhibitory pathway causes lethal hyperthermia via dysregulated increases in thermogenesis and skin vasoconstrictor activity (*8*, *9*). Therefore, the POA neuron group for this tonic inhibitory control has long been sought. Our study shows strong evidence that POA^{EP3R} neurons provide tonic GABAergic inhibitory signaling to sympathoexcitatory efferent pathways as a fundamental determinant of body temperature for thermal homeostasis and fever (Fig. 8).

Earlier studies examined the effects on T_{core} of selective stimulation and inhibition of VGLUT2-expressing and VGAT-expressing POA neurons in mice (*34*–*37*). However, both glutamatergic and GABAergic populations in the POA are composed of heterogeneous subgroups with different projection properties (i.e., interneurons and projection neurons) and different roles in thermoregulation (*3*, *4*), and therefore, the manipulations of the entire VGLUT2- or VGAT-expressing population of POA neurons have not permitted dissection of the thermoregulatory neural circuit. With efforts to classify POA neuron subgroups, recent studies have identified various genetic markers: pituitary adenylate cyclase-activating polypeptide, brain-derived neurotrophic factor, leptin receptor, galanin, neuronal nitric oxide synthase, pyroglutamylated RFamide peptide, estrogen receptor α, and opsin 5 (*35*, *38*–*45*). Stimulation of any of these POA neuron subgroups results in hypothermia at room temperature, and some of them induce torpor-like severe hypothermia with T_{core} reduced to room temperature (*42*–*45*). However, none of them elicits obvious hyperthermia when inhibited, although some subgroups show partial overlap with POA^{EP3R} neurons (*17*, *43*). Therefore, these POA neuron subgroups likely mediate heat defense, and some of them may drive torpor when mice are hungry in cold environments, but they seem unlikely to function for cold defense or fever. Another group of POA neurons expressing bombesin-like receptor 3 (BRS3) is activated by cooling of mice and drives cold-defensive responses but does not mediate lipopolysaccharide (LPS)–induced fever (*32*). Chemogenetic inhibition of BRS3-expressing POA neurons elicits only a modest decrease (0.5°C) in T_{core} (*32*). In notable contrast, the present study showed that POA^{EP3R} neurons, which are activated by heat exposure and inhibited by PGE_2, bidirectionally control T_{core}. The chemogenetic stimulation of POA^{EP3R} neurons reduced T_{core} by 1.9°C, which was less severe than the torpor-like hypothermia induced by the other POA neuron subgroups. Therefore, POA^{EP3R} neurons constitute an as-yet-unreported, unique, and pivotal group of thermoregulatory POA neurons that mediates not only fever development but also thermal homeostasis in both hot and cold environments.

A recent Fos mapping study identified a group of LPS-activated inhibitory neurons in the ventromedial preoptic nucleus (VMPO^{LPS} neurons) (*46*). These neurons are activated by LPS-evoked immune signaling, including PGE_2-EP2R signaling, but do not express EP3R (*46*). Chemogenetic stimulation of VMPO^{LPS} neurons increases body temperature and decreases food intake, whereas ablation of them eliminates LPS-induced fever, indicating that these neurons mediate sickness symptoms including fever (*46*). Given the indispensable role of the preoptic EP3R in LPS-induced fever (*16*), PGE_2 probably needs to act on both POA^{EP3R} and VMPO^{LPS} neurons to trigger fever. VMPO^{LPS} neurons are not involved in basal thermoregulation but seem to innervate thermoregulatory neurons in the MnPO (*46*). Therefore, during infection, an inflammation-driven ad hoc input from VMPO^{LPS} neurons, together with a direct PGE_2 action on POA^{EP3R} neurons, may inhibit POA^{EP3R} neurons to attenuate the tonic descending inhibition of sympathetic outflow, leading to fever development.

Because POA^{EP3R} neurons exhibited a low level of Fos expression during exposure to room temperature, we could not detect cold exposure–induced inhibition of these neurons by monitoring Fos, which is an immediate-early transcription factor expressed in response to intense neuronal excitation involving an elevation of intracellular Ca^{2+} (*47*). However, chemogenetic inhibition of POA^{EP3R} neurons at room temperature elicited BAT thermogenesis and hyperthermia. This result indicates that POA^{EP3R} neurons under room temperature conditions exhibit a certain level of tonic firing that does not involve Ca^{2+} influx leading to Fos expression, and inhibition of this tonic activity, probably by a cold-sensory input from the skin through the lateral parabrachial nucleus (*6*), elicits cold-defensive thermoregulatory responses including BAT thermogenesis. Future electrophysiological recordings from POA^{EP3R} neurons will allow us to directly measure their activity responses to cutaneous thermosensory inputs and to determine whether these neurons have intrinsic thermosensitivity as warm-sensitive neurons that sense local brain tissue temperature (*48*).

The increased activity of POA^{EP3R} neurons by heat exposure was reduced by PGE_2. Although the EP3R is mostly coupled to G_i in cultured cells (*18*), it has been unknown how PGE_2 alters POA neuronal activities through the EP3R to trigger fever. The present results demonstrate that PGE_2 inhibits POA^{EP3R} neuronal activity to elevate T_{core}, and our correlation analysis between Fos expression and T_{core} predicted that suppression of all POA^{EP3R} neurons by PGE_2 would increase T_{core} up to 42.1°C, close to the typical upper

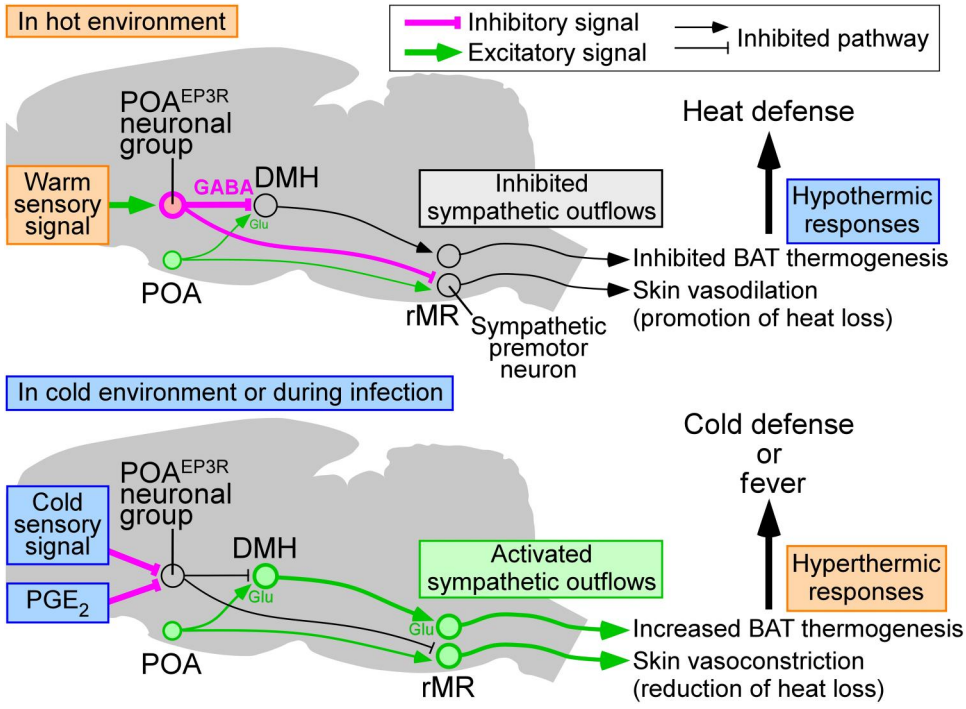

Fig. 8. A model of the central circuit mechanism for thermoregulation and fever. This scheme illustrates how tonic inhibitory signaling from POA^{EP3R} neurons bidirectionally controls T_{core} for thermal homeostasis and development of fever. In a hot environment (**top**), cutaneous warm-sensory signals activate POA^{EP3R} → DMH projection neurons, which then provide strong GABAergic inputs to sympathoexcitatory DMH neurons to inhibit the sympathetic efferent pathways to BAT and cardiovascular organs. Another separate POA^{EP3R} neuronal subgroup that innervates the rMR may also be activated and inhibit sympathetic outflow to skin vasoconstrictors to elicit skin vasodilation. The inhibitory signaling from POA^{EP3R} neurons dominates over glutamatergic excitatory inputs from the POA (and from other as-yet-unidentified brain regions) to the DMH and rMR. The elicited hypothermic effector responses, including inhibition of heat production and promotion of heat loss, defend T_{core} in the hot environment. In a cold environment or during infection (**bottom**), cutaneous cold-sensory signals or PGE_2 inhibits POA^{EP3R} → DMH projection neurons. Consequently, the GABAergic tonic signaling from POA^{EP3R} neurons is attenuated, and thereby, the glutamatergic inputs to the DMH and rMR can drive sympathetic outflows to BAT, skin vasoconstrictors, and cardiovascular organs. These sympathetic outputs drive hyperthermic responses, such as increased BAT thermogenesis and skin vasoconstriction, for the defense of T_{core} in the cold environment or for the development of fever.

limit of fever (*49*). The view that the G_i-mediated reduction of the intracellular cAMP levels in POA^{EP3R} neurons inhibits their neural activity and thereby mediates the febrile action of PGE_2 is consistent with previous findings that intracerebroventricular injection of PGE_2 reduces cAMP levels in the POA and that blockade of cAMP degradation in the POA impairs PGE_2-induced fever (*50*).

An intriguing finding in this study is the discrepant expressions of the transmitter markers in the cell bodies and axon terminals of POA^{EP3R} neurons. The glutamatergic neuronal marker, VGLUT2 mRNA, was more prevalently expressed in their cell bodies than the GABAergic marker, GAD67 mRNA, consistent with a recent result that ablation of the *Ptger3* gene in Cre-expressing cells in VGLUT2-Cre mice blunted the febrile response to LPS (*17*). However, our anterograde tracing from POA^{EP3R} neurons combined with immunohistochemistry revealed that DMH axon terminals of POA^{EP3R} neurons predominantly contain VGAT proteins but few VGLUT2 proteins, indicating that these neurons release GABA, rather than glutamate, in the DMH. The DMH contains sympathoexcitatory neurons that innervate the rMR to drive cold-defensive, febrile, and stress responses (*11*, *12*, *21*, *22*, *25*, *51*), and we found that cell bodies of rMR-projecting DMH neurons were more often in close contact with VGAT-containing axons of POA^{EP3R} neurons than VGLUT2-containing axons. Because these vesicular transporter proteins, but not mRNAs, are the entities that function for neurotransmission, the abundant presence of VGAT proteins in those axon terminals is a stronger evidence for the transmitter properties of POA^{EP3R} neurons than the results based on gene transcripts. Our immunohistochemical procedure was validated by the results that VGAT-immunoreactive puncta were colabeled with other antibodies raised against different epitopes on the VGAT protein and that our VGLUT2 immunohistochemistry successfully visualized glutamatergic terminals in palGFP-labeled thalamocortical axons. Furthermore, many VGAT-immunoreactive puncta of POA^{EP3R} neuronal axons in the DMH were accompanied by synaptophysin and GAD67 immunoreactivities, indicating that these VGAT-immunoreactive puncta are presynaptic structures that can both produce and release GABA. These immunohistochemical observations are supported by our electrophysiological evidence that POA^{EP3R} neuron–derived axons predominantly form GABAergic synapses onto DMH neurons. Bilateral chemogenetic inhibition of transmitter release from POA^{EP3R} → DMH axon terminals elicited BAT thermogenesis and tachycardia. Together, these results provide the central thermoregulatory and febrile mechanisms, in which POA^{EP3R} neurons directly innervate DMH → rMR sympathoexcitatory neurons via tonic GABAergic inputs, and attenuation of the tonic GABAergic signaling by cutaneous cold-

sensory inputs to, or by a PGE_2 action on, POA^{EP3R} neurons disinhibits the sympathoexcitatory neurons to drive thermogenic and cardiovascular responses (Fig. 8).

Our observation that EP3Rs are expressed by both VGLUT2 mRNA–expressing and GAD67 mRNA–expressing POA neuronal groups is consistent with the recent single-cell/nucleus RNA sequencing data showing *Ptger3* mRNA expression in both "excitatory" and "inhibitory" POA cell clusters (*52*, *53*). The abundant GABAergic axons of POA^{EP3R} → DMH neurons might be provided exclusively by the GAD67 mRNA–expressing population. The GAD67 mRNA–expressing POA^{EP3R} neurons probably also express VGAT, because *Ptger3* mRNA is expressed in some inhibitory clusters expressing both *Slc32a1* (VGAT) and *Gad1* (GAD67) mRNAs (*53*), and we found GAD67 immunoreactivity in many VGAT-immunoreactive puncta of POA^{EP3R} → DMH axons. However, DMH-projecting POA^{EP3R} neurons predominantly express VGLUT2 mRNA (fig. S3G). Therefore, VGLUT2 mRNA–expressing POA^{EP3R} neurons also likely produce the proteins required to be GABAergic, such as VGAT and GAD67. Double fluorescence in situ hybridization for VGLUT2 and GAD67 mRNAs combined with EP3R immunohistochemistry could have allowed us to determine the extent to which these two mRNAs are coexpressed in POA^{EP3R} neurons, but it was technically difficult. Note that even excitatory POA cell clusters (expressing VGLUT2 mRNA) express very low levels of VGAT mRNA (*52*, *53*) and that mRNA transcript levels by themselves are not sufficient to predict their protein product levels in many types of cells (*54*). Therefore, in VGLUT2 mRNA–expressing POA^{EP3R} neurons, sufficient amounts of these GABAergic presynaptic proteins could be translated from low levels of mRNA transcripts. Furthermore, these mRNAs may be targeted to axon terminals for local translation into those GABAergic presynaptic proteins (*55*, *56*), and these axonal mRNAs leaving cell bodies soon after transcription would be difficult to be detected by in situ hybridization or single-cell/nucleus RNA sequencing. The present results provide a potential caveat that VGLUT2 gene transcripts in cell bodies, particularly in POA neurons, are not a reliable marker for glutamatergic neurons.

Another interesting finding is the increase in VGAT-immunoreactive puncta of POA^{EP3R} → DMH axons following chronic heat exposure. This observation leads us to hypothesize a heat adaptation mechanism, in which POA^{EP3R} neurons during chronic heat exposure form more GABAergic inhibitory synapses onto sympathoexcitatory DMH neurons to increase the ability to tolerate heat stress. The concomitant reduction of POA^{EP3R} → DMH axon swellings lacking VGAT and VGLUT2 suggests that these empty axons serve as a reserve, which is to be installed with GABAergic presynaptic machinery when necessary to tolerate heat. The local translation in axon terminals may be involved in the installation with GABAergic presynaptic proteins, and how chronic heat exposure triggers this adaptation mechanism is an interesting question for future research.

In the present study, local chemogenetic inhibition of transmitter release from POA^{EP3R} → DMH axon terminals potentiated BAT thermogenic, metabolic, and pressor responses evoked by glutamatergic stimulation of DMH neurons. This result indicates that the POA^{EP3R} → DMH tonic GABAergic signal is a critical determinant of the E/I balance that regulates the excitability of sympathoexcitatory DMH neurons whose activation leads to the elevation of T_{core}. The hyperthermia evoked by chemogenetic inhibition of POA^{EP3R} neurons in awake rats (Fig. 6D) suggests that sympathoexcitatory DMH neurons receive a certain level of glutamatergic inputs in awake conditions under room temperature but cannot actively generate action potentials until concurrent tonic GABAergic inputs from POA^{EP3R} neurons are attenuated by cold-sensory inputs or PGE_2 (Fig. 8). Consistent with this view, robust (bilateral) chemogenetic suppression of POA^{EP3R} → DMH transmission by itself elicited BAT thermogenesis and tachycardia. Therefore, the POA^{EP3R} → DMH GABAergic signaling, whose tone is altered by cutaneous and central thermosensory signals, makes a major contribution to setting the control range of T_{core}. The glutamatergic inputs from the POA to sympathoexcitatory DMH neurons may also be regulated by thermosensory signals (activated by cold) (*30*–*32*). However, sympathoexcitatory DMH neurons also likely receive temperature-independent, intense excitatory signals from other brain sites perhaps located caudal to the POA, because a complete disruption of fibers descending from the POA in rats elicits intense BAT thermogenesis and cutaneous vasoconstrictor activity leading to hyperthermia (*8*, *9*).

Thermoregulation and fever involve various effector responses. The present results show that the POA^{EP3R} → DMH pathway controls BAT thermogenesis and accompanying cardiovascular responses. This finding is consistent with the notion that DMH neurons mediate BAT thermogenesis and cardiovascular responses for fever and cold defense (*12*, *22*, *24*). The POA^{EP3R} → DMH pathway is also likely to control shivering thermogenesis, because the POA and DMH mediate cold-defensive and febrile shivering (*11*). Our finding that stimulation of POA^{EP3R} neurons elicits cutaneous vasodilation (Fig. 6, H and I) indicates that these neurons regulate cutaneous vasomotion for thermal homeostasis. However, the DMH does not mediate cutaneous vasoconstriction for fever or cold defense (*9*), although it does mediate psychological stress–induced cutaneous vasoconstriction (*51*). Cutaneous vasomotion for basal thermal homeostasis and fever is likely controlled by a pathway from POA^{EP3R} neurons to the rMR bypassing the DMH (Fig. 8) (*10*, *13*, *30*), which was visualized in the present anterograde tracing (fig. S5J). The subgroups of POA^{EP3R} → DMH and POA^{EP3R} → rMR projection neurons do not overlap (*13*). Further studies are awaited to determine how these two descending pathways from POA^{EP3R} neurons cooperate to regulate multiple effector organs in a coordinated manner for thermoregulation and fever development.

MATERIALS AND METHODS

Generation of *Ptger3*-tTA BAC transgenic rats

We modified a bacterial artificial chromosome (BAC) clone (CH230-35G1) from a female BN/SsNHsd/MCW rat genomic BAC library (BACPAC Resources) that consisted of a pTARBAC2.1 vector and a genomic DNA fragment (~243 kb) containing the *Ptger3* gene. To replace the loxP site in the BAC vector with a homing endonuclease (I–Sce I) recognition site, we first generated the pTARBAC1H vector from the pTARBAC1 vector (BACPAC Resources) by replacing the loxP site with the I–Sce I site and by deleting the loxP511 site. The pTARBAC2.1 backbone of the BAC clone was then replaced with the pTARBAC1H backbone by Red/ET recombination (Counter Selection BAC modification kit; Genebridges, Heidelberg, Germany) using an appropriate rpsL/neo cassette according to the manufacturer's manual. The

recombined BAC DNA was further subjected to another Red/ET recombination to insert a DNA cassette (989 base pairs) consisting of tTA Advanced (tTAad), an improved version of tTA, and bovine growth hormone polyadenylation sequence (BGH) at immediately 3′ to the start ATG codon of the *Ptger3* gene (fig. S4A).

The recombined *Ptger3*-tTA-BGH BAC was purified with a NucleoBond BAC 100 kit (Macherey-Nagel, Düren, Germany), and the DNA was digested for 1 hour with I–Sce I (New England Biolabs, Beverly, MA) at 37°C. The linearized BAC DNA was then injected into the pronuclei of Sprague-Dawley rat zygotes (Japan SLC, Shizuoka, Japan). The zygotes were transferred into pseudo-pregnant female rats, and 63 pups were obtained. Genomic DNAs of 61 weaned pups (2 pups died before weaning) were collected from their tails with a DNeasy tissue kit (QIAGEN, Valencia, CA). Six *Ptger3*-tTA BAC transgenic founder rats were identified by polymerase chain reaction (PCR) for the presence of the tTAad-BGH insert, 5′ end (T7 arm), and 3′ end (Sp6 arm) of the linearized BAC DNA by PCR (fig. S4B). To further evaluate the selectivity of the reporter gene expression in these founder lines, we injected AAV-TRE-palGFP into the POA and performed double immunostaining for GFP and EP3R (see below). One of the founder lines, which exhibited the highest specificity of palGFP expression in POA^{EP3R} neurons (line ID: 101001-09-5; Fig. 4, A and B), was chosen and used in the present study. On the basis of the inheritance pattern of the transgene, in this founder line, the BAC transgene was found to be located in the X chromosome, but the transgenic rats were fertile with no obvious abnormalities. The transgenic line was maintained in heterozygotes on a Sprague-Dawley genetic background, and transmission of the transgene to offsprings was monitored by PCR.

Animals

Male Sprague-Dawley rats (200 to 500 g; Japan SLC) and male *Ptger3*-tTA rats (100 to 500 g) were used. They were housed two or three to a cage with ad libitum access to food and water in a room air-conditioned at 25° ± 2°C with 50 ± 15% humidity under a standard 12-hour light/12-hour dark cycle (lights on from 7:00 a.m. to 7:00 p.m.) before being used for surgery or experiments. All procedures conform to the guidelines of animal care by the Division of Experimental Animals, Nagoya University Graduate School of Medicine, and were approved by the Nagoya University Animal Experiment Committee (#M220097-002). This study used males because the effects of the female estrus cycle on thermoregulation and fever could make the interpretation of experimental results difficult. Sample sizes (i.e., numbers of animals used) for experimental groups were determined on the basis of our experience and standards in the field (*6*, *21*, *22*) to be the minimum necessary to obtain statistical power. Animals were randomly allocated to each experimental group.

AAV vectors

Production of AAV vectors followed our established procedure (*51*, *57*). For the production of pAAV2-TRE-palGFP, a palGFP DNA cassette was amplified with a PCR method using pAAV-CMV-palGFP (*25*) as a template together with primers containing a 5′-Bam HI site and a 3′-Mlu I site. After digestion with these restriction enzymes, this cassette was inserted into the multicloning site of pENTR1A-TRE (*58*) between the Bam HI/Mlu I sites. Similarly, for the production of pAAV2-TRE-mCherry-T2A-$hM4Di^{nrxn}$, an mCherry-T2A-$hM4Di^{nrxn}$ cassette was PCR-amplified using CAG::mCherry-2a-hM4Dnrxn (Addgene, #52523; donated by S. Sternson) as a template with primers containing a 5′-Bam HI site and a 3′-Mlu I site and then inserted into pENTR1A-TRE. For the production of pAAV2-TRE-hM3Dq-mCherry, an hM3Dq-mCherry cassette was PCR-amplified using pAAV-hSyn-DIO-hM3Dq-mCherry (Addgene, #44361; donated by B. Roth) as a template with primers containing a 5′-Mlu I site and a 3′-Eco RI site and then inserted into pENTR1A-TRE between the Mlu I/Eco RI sites. The produced entry vectors—pENTR1A-TRE-palGFP, pENTR1A-TRE-mCherry-T2A-$hM4Di^{nrxn}$, and pENTR1A-TRE-hM3Dq-mCherry—were subjected to homologous recombination using LR Clonase II with the destination vector, pAAV2-DEST(r) (*59*), to produce pAAV2-TRE-palGFP, pAAV2-TRE-mCherry-T2A-$hM4Di^{nrxn}$, and pAAV2-TRE-hM3Dq-mCherry. For the production of pAAV2-TRE-ChIEF-EYFP, a ChIEF-EYFP cassette was produced by an overlap PCR method using pAAV-CMV-ChIEF-tdTomato (*25*) and pLenti-CaMKIIα-eArchT3.0-EYFP (Addgene, #35513; donated by K. Deisseroth) as templates together with primers containing a 5′-Sal I site and a 3′-Eco RV site. After digestion with these restriction enzymes, this cassette was inserted into the Sal I/Eco RV sites of pAAV-PTRE-tight-flex-hM3Dq-mCherry-WPRE-pA (Addgene, #115161; donated by W. Wisden) to replace the flex-hM3Dq-mCherry cassette and thereby to produce pAAV2-TRE-ChIEF-EYFP.

The pAAV2 vectors were used for the production and purification of AAV2/1-TRE-palGFP, AAV2/1-TRE-mCherry-T2A-$hM4Di^{nrxn}$, AAV2/1-TRE-hM3Dq-mCherry, and AAV2/1-TRE-ChIEF-EYFP according to our methods (*51*, *57*). The final titrations were 1.2×10^{13} genome copy (GC)/ml (AAV-TRE-palGFP), 1.1×10^{13} GC/ml (AAV-TRE-mCherry-T2A-$hM4Di^{nrxn}$), 1.3×10^{13} GC/ml (AAV-TRE-hM3Dq-mCherry), and 6.7×10^{14} GC/ml (AAV-TRE-ChIEF-EYFP). AAV-TRE-hM3Dq-mCherry was diluted 50-fold with 0.9% saline before intracranial injection.

Stereotaxic injection

Rats were anesthetized with a combination anesthetic [medetomidine hydrochloride (0.15 mg/kg), midazolam (2.0 mg/kg), and butorphanol tartrate (2.5 mg/kg); intraperitoneally or subcutaneously] following gas anesthesia with 3% isoflurane and were positioned in a stereotaxic apparatus. With this anesthesia, no rats exhibited any sign of pain or discomfort during surgery or postoperative recovery. A glass micropipette filled with a solution containing AAV, CTb conjugated with Alexa Fluor 488 (Alexa488) or Alexa647 (1 mg/ml; C22841 and C34778, Thermo Fisher Scientific), or FG (4% solution dissolved in 0.9% saline; Fluorochrome, Denver, CO) was perpendicularly inserted into the POA (AAV), anterior midline thalamus (AAV), DMH (CTb or FG), or rMR (FG). The solution was pressure-ejected using a Picospritzer III (Parker, Hollis, NH), and the micropipette remained for 5 min after injection before it was withdrawn. The following are AAV injections into the POA targeted at three sites (150 nl per site): MnPO (0.3 mm rostral to bregma, on the midline, and 7.2 mm ventral to the brain surface) and MPA (0.1 mm rostral to bregma, 0.6 to 0.7 mm left and right to the midline, and 7.8 mm ventral to the brain surface). AAV injection into the anterior midline thalamus (200 nl) was made at the following coordinates: 2.0 mm caudal to bregma, on the midline, and 5.0 to 5.5 mm ventral to the brain surface. CTb injection (250 nl) was made unilaterally into the DMH (3.1 mm caudal to bregma,

0.4 to 0.8 mm lateral to the midline, and 8.5 mm ventral to the brain surface). FG injections into the DMH were made at the same coordinates but bilaterally (50 nl per site). FG injection into the rMR (80 nl) was made at the following coordinates: 2.8 mm caudal to the interaural line, on the midline, and 9.6 mm ventral to the brain surface. After the injection, all incisions were sutured and disinfected with iodine, and ampicillin sodium (0.2 ml, 125 mg/ml) and atipamezole hydrochloride (250 μg/kg) solutions were injected into femoral muscles. The rats were housed 7 to 10 days (8 to 9 weeks for slice patch-clamp recordings) under regular health check until subsequent procedure or experiments.

Cold and heat exposure

Cold and heat exposure of rats was performed in a climate chamber (*23*), with the standard light/dark control as described above. Rats were individually placed in plastic cages with wire mesh lids with ad libitum food and water. For acute exposure experiments, the cages were placed in the climate chamber air-conditioned at 24°C overnight to acclimatize the rats to the chamber, and then they were exposed to 4°, 24°, or 36°C for 2 hours (approximately between 9:00 a.m. and 12:00 p.m.). The duration of the cold and heat exposure was determined on the basis of our previous study, in which the expression of Fos protein in hypothalamic neurons was immunohistochemically detected 1 to 2 hours after the initiation of exposure to stress (*25*). For chronic exposure, rats were exposed to 10°, 25°, or 34°C for 16 days (10°C) or 14 days (25° and 34°C), except short periods of time for regular health check and cage maintenance. The temperatures for chronic cold and heat exposure were milder than those for the acute exposure, because some rats could not survive in our preliminary experiments. Immediately after the exposure, the rats were anesthetized and transcardially fixed for histological analyses as described below.

Immunohistochemistry

Immunohistochemical procedures followed our previous studies (*15*, *23*). Rats were anesthetized with the combination anesthetic described above following gas anesthesia with 3% isoflurane and transcardially perfused with saline and then with 4% formaldehyde in 0.1 M phosphate buffer (pH 7.4). The brain was removed, postfixed in the fixative at 4°C for 2 to 3 hours, and then cryoprotected in a 30% sucrose solution longer than overnight. The tissue was cut into 30-μm-thick frontal sections on a freezing microtome. The primary antibodies used are anti-EP3R rabbit antibody (1 μg/ml) (*14*, *15*), anti-Fos goat antibody (1:1000; sc-52G, Santa Cruz Biotechnology), anti-CTb goat serum (1:5000; #703, List Biological Laboratories), anti-GFP mouse antibody (1:200; A11120, Thermo Fisher Scientific), anti-GFP rabbit antibody (0.5 μg/ml) (*60*), anti-VGAT guinea pig serum (1:1000; 131004, Synaptic Systems), anti-VGLUT2 rabbit antibody (0.5 μg/ml) (*61*), anti-GAD67 mouse antibody (1:300; MAB5406, Sigma-Aldrich), anti-synaptophysin mouse antibody (1:1000; S5768, Sigma-Aldrich), and anti-monomeric red fluorescent protein (mRFP) guinea pig antibody (1 μg/ml) (*62*). The anti-mRFP guinea pig antibody and the anti-GFP mouse antibody showed cross-reactivity to mCherry and EYFP, respectively. VGAT immunohistochemistry using the anti-VGAT guinea pig serum (epitope: amino acids 2 to 115 on rat VGAT) was validated by costaining with anti-VGAT mouse antibody (1:200; 131011, Synaptic Systems; epitope: amino acids 75 to 87 on rat VGAT) and anti-VGAT rabbit antibody (1:200; VGAT11-A, Alpha Diagnostics; epitope: 17 amino acids of the C terminus of rat VGAT) (fig. S6E). The specificity of all the in-house antibodies was confirmed by antigen absorption, immunoblotting, and/or immunostaining of a genetically expressed antigen (see the accompanying references). The specificity of the commercially available antibodies was confirmed by the manufacturers, and the immunohistochemical performance of the antibodies has been reported in previous studies, which can be searched at the Antibody Registry (https://antibodyregistry.org).

For double immunofluorescence staining for EP3R and Fos, sections were incubated with anti-EP3R rabbit antibody and anti-Fos goat antibody overnight at 4°C and then with Alexa594-conjugated donkey antibody to goat immunoglobulin G (IgG) (10 μg/ml; A11058, Thermo Fisher Scientific) and biotinylated donkey antibody to rabbit IgG (1:100; AP182B, Merck Millipore) for 1 hour at room temperature. After rinsing, these sections were further incubated with avidin-biotinylated peroxidase complex (ABC; 1:50; PK-6100, Vector Laboratories) for 1 hour, and then EP3R immunoreactivity was visualized by reaction with fluorescein isothiocyanate (FITC)–conjugated tyramide (1:50; SAT701001KT; Tyramide Signal Amplification FITC Systems, PerkinElmer) for 3 min. For double immunofluorescence staining for EP3R and mCherry, mCherry was detected by anti-mRFP guinea pig antibody and Alexa594-conjugated goat antibody to guinea pig IgG (10 μg/ml; A11076, Thermo Fisher Scientific). For double immunofluorescence staining for EP3R and EYFP, sections were incubated with anti-EP3R rabbit antibody and anti-GFP mouse antibody (for detection of EYFP) overnight and then with Alexa488-conjugated goat antibody to mouse IgG (10 μg/ml; A11029, Thermo Fisher Scientific) and biotinylated donkey antibody to rabbit IgG (1:100) for 1 hour. The sections were further incubated with ABC (1:50) for 1 hour, and then EP3R immunoreactivity was visualized by reaction with Cy3-conjugated tyramide (1:50; SAT704A001EA, Akoya Biosciences) for 6 min. In case of counterstaining of cell nuclei, immunostained sections were incubated with 4′,6-diamidino-2-phenylindole (DAPI; 1:1000; D523, Dojindo, Kumamoto, Japan) for 30 min.

For triple immunolabeling in palGFP-labeled axons, brain sections were incubated overnight with a mixture of anti-GFP mouse antibody, anti-VGAT guinea pig serum, and anti-VGLUT2 rabbit antibody; a mixture of anti-GFP rabbit antibody, anti-VGAT guinea pig serum, and anti-GAD67 mouse antibody; a mixture of anti-GFP rabbit antibody, anti-VGAT guinea pig serum, and anti-synaptophysin mouse antibody; or a mixture of anti-VGAT guinea pig serum, anti-VGAT mouse antibody, and anti-VGAT rabbit antibody. The sections were then incubated for 2 hours with an appropriate combination of the secondary antibodies (10 μg/ml for each): Alexa488-conjugated goat antibody to mouse IgG (A11029, Thermo Fisher Scientific), Alexa488-conjugated goat antibody to rabbit IgG (A11034, Thermo Fisher Scientific), Alexa568-conjugated goat antibody to guinea pig IgG (A11075, Thermo Fisher Scientific), Alexa647-conjugated goat antibody to rabbit IgG (A21245, Thermo Fisher Scientific), and Alexa647-conjugated goat antibody to mouse IgG (A21236, Thermo Fisher Scientific). Immunoreactivity of the anti-VGAT rabbit antibody was detected by incubation with biotinylated donkey antibody to rabbit IgG followed by incubation with streptavidin-conjugated Alexa647 (1:400; S21374, Thermo Fisher Scientific).

Fluorescence in situ hybridization

Rats were anesthetized with the combination anesthetic described above following gas anesthesia with 3% isoflurane and transcardially perfused with 4% formaldehyde in 0.1 M phosphate buffer (pH 7.4). The brains were postfixed in the fixative at 4°C for 3 days and then cryoprotected in a 30% sucrose solution for at least 2 days. The tissues were cut into 35-μm-thick frontal sections on a freezing microtome in a ribonuclease-free environment. These sections were blocked in a hybridization buffer [4.95× SSC, 1.98% Blocking Reagent (11096176001, Roche), 49.5% formamide, 0.099% *N*-lauroylsarcosine (NLS), and 0.099% SDS] at 60°C for 1 hour and then incubated with digoxigenin-labeled rat GAD67 or mouse VGLUT2 antisense RNA probe (1 μg/ml) (*10*, *63*) in this buffer at 60°C for 20 to 22 hours. The sections were washed with 2× SSC containing 50% formamide and 0.1% NLS at 60°C for 20 min twice and then further washed with the following solutions at 37°C for 20 min twice for each solution: (i) 2× SSC containing 0.1% NLS and (ii) 0.2× SSC containing 0.1% NLS. After rinsing with TS7.5 solution [0.1 M tris-HCl and 0.15 M NaCl (pH7.5)] at room temperature for 5 min, the sections were blocked in TS7.5 containing 1% Blocking Reagent for 1 hour and then incubated with alkaline phosphatase–conjugated anti-digoxigenin sheep antibody (1:1000; 11093274910, Roche) and anti-EP3R rabbit antibody in this blocking solution overnight at 4°C. In case of detecting Fos, anti-Fos goat antibody was added to this antibody cocktail. After rinsing with TS7.5 containing 0.05% Tween 20 (TNT) for 5 to 10 min twice, these sections were incubated with biotinylated donkey antibody to rabbit IgG in TS7.5 containing 1% Blocking Reagent for 1 hour at room temperature. In case of detecting Fos immunoreactivity, Alexa647-conjugated donkey antibody to goat IgG (10 μg/ml; A21447, Thermo Fisher Scientific) was added to this solution. After rinsing with TNT for 5 min twice, the sections were incubated with TS7.5 containing ABC (1:50) for 1 hour. After washing with TNT for 10 min twice and then with TS8.0 solution [0.1 M tris-HCl, 0.1 M NaCl, and 10 mM $MgCl_2$ (pH 8.0)] for 10 min twice, the sections were incubated with an HNPP/Fast Red TR solution (11758888001, Roche) at room temperature for 2.5 hours. After rinsing with TS7.5, these sections were further incubated with FITC-conjugated tyramide as described above. These sections were rinsed with TS7.5 and then soaked in ice-cold TS8.0 to be mounted onto glass slides. The slides were dried in the dark and then briefly soaked into TS8.0 to be coverslipped with CC/Mount (Diagnostic BioSystems). In our preliminary experiments, we confirmed that the mouse VGLUT2 antisense probe showed hybridization signals in the rat brain, consistent with reported VGLUT2 mRNA distribution (*63*).

For fluorescence in situ hybridization combined with EP3R and CTb immunohistochemistry, hybridization signals were detected using peroxidase instead of alkaline phosphatase. Sections after the posthybridization washing and blocking steps were incubated with peroxidase-conjugated anti-digoxigenin sheep antibody (1:1000; 11207733910, Roche) in TS7.5 containing 1% Blocking Reagent at 4°C for overnight. After rinsing with TS7.5, the sections were incubated with Cy3-conjugated tyramide (1:50) in Amplification Diluent (SAT704A001KT, PerkinElmer) supplemented with 0.00014% H_2O_2 and 4% polyvinyl alcohol (molecular weight of 31,000 to 50,000; 363138, Sigma-Aldrich) for 6 hours at room temperature. After washing with TNT for 30 min, the sections were incubated in phosphate-buffered saline (PBS) containing 3% H_2O_2 for 10 min at room temperature to block the peroxidase activity. The sections were thoroughly washed with TNT and with TS7.5 and then incubated with anti-EP3R rabbit antibody and anti-CTb goat serum in TS7.5 containing 1% Blocking Reagent at 4°C for overnight. After rinsing with TNT, the sections were further incubated with Alexa647-conjugated donkey antibody to goat IgG (for rats injected with Alexa647-conjugated CTb) or Alexa488-conjugated donkey antibody to goat IgG (10 μg/ml; A11055, Thermo Fisher Scientific; for rats injected with Alexa488-conjugated CTb) in TS7.5 containing 1% Blocking Reagent at room temperature for 1 hour. The sections were blocked with 10% normal goat serum in TS7.5 for 30 min and then incubated with biotinylated donkey antibody to rabbit IgG in TS7.5 containing 1% Blocking Reagent and 10% normal goat serum for 1 hour at room temperature. The sections were further incubated with ABC in TS7.5 for 1 hour, and then EP3R immunoreactivity was visualized by reaction with FITC-conjugated tyramide as described above (for rats injected with Alexa647-conjugated CTb) or with Alexa647-conjugated tyramide (1:50 to 1:100; B40958, Thermo Fisher Scientific) in PBS containing 0.0002 to 0.0015% H_2O_2 for 5 min (for rats injected with Alexa488-conjugated CTb). The sections were mounted on glass slides and dried in the dark at 4°C overnight.

Microscopy and histological quantification

Stained sections were mounted on glass slides and coverslipped with 50% glycerol/50% PBS containing 2.5% triethylenediamine (or CC/Mount for Fast Red staining as mentioned above). The sections were observed under an epifluorescence microscope (Eclipse 80i, Nikon) or a confocal laser scanning microscope (TCS SP8, Leica). FG was detected with the fluorescence of the tracer. Confocal images were acquired using the *z*-stacking function at an interval of 2.5 μm for cell body images in the POA or 1.8 μm for axon images in the DMH and tiled with a LAS X software (Leica).

Labeled cell bodies in EP3R-immunoreactive areas (fig. S1A) were mapped in every sixth section through the POA [approximate rostrocaudal levels: bregma +0.4 mm to −0.3 mm; representative examples are shown in Fig. 1C and figs. S1 (C and E), S2, and S3 (A, C, and D)] and manually counted. The quantification was made bilaterally, except for CTb-labeled cell bodies (Fig. 3H and fig. S3G), which were counted in the MnPO and the MPA ipsilateral to the CTb injection. For quantification of the presynaptic structures of the DMH-projecting axons of POA^{EP3R} neurons, confocal *z*-stack images covering the entire DMH were acquired bilaterally at two different rostrocaudal levels (five sections apart) including bregma −3.1 mm (fig. S7D). For quantification of thalamocortical axon terminals, confocal *z*-stack images of the area 2 of the cingulate cortex were acquired unilaterally from one section. After tiling these *z*-stack images, we counted puncta immunoreactive for the presynaptic vesicular transporter proteins, VGAT and VGLUT2, in palGFP-labeled axons, which were regarded as presynaptic sites that release GABA and glutamate, respectively. To quantify palGFP-labeled axon swellings that contained neither VGAT- nor VGLUT2-immunoreactive profile (empty swellings), we counted axon swellings that were at least 1.5 times thicker than the adjoining axon shaft.

Slice patch-clamp recordings

Ptger3-tTA rats at 8 to 9 weeks after injection of AAV-TRE-ChIEF-EYFP into the POA were anesthetized with 5% isoflurane and perfused transcardially with an ice-cold cutting solution containing the

following: 96 mM *N*-methyl-D-glucamine, 2.5 mM KCl, 1.25 mM NaH_2PO_4, 25 mM $NaHCO_3$, 20 mM Hepes, 25 mM D-glucose, 12 mM *N*-acetyl-L-cysteine, 5 mM Na ascorbate, 2 mM thiourea, 3 mM Na pyruvate, 3 mM myo-inositol, 0.01 mM taurine, 0.5 mM $CaCl_2$, and 10 mM $MgSO_4$, which was saturated with 95% O_2 and 5% CO_2 (300 to 310 mOsm). The pH of the solution was titrated to 7.2 to 7.3 with HCl. The rats were decapitated, and then the brains were removed. Transverse hypothalamic slices (300 μm thick) containing the DMH were prepared with a tissue slicer (DTK-1000, Dosaka EM, Kyoto, Japan) in the ice-cold cutting solution. The slices were first incubated in a holding chamber containing the cutting solution at 36°C for 15 min and then transferred to another chamber containing a recovery solution composed of 94 mM NaCl, 2.5 mM KCl, 1.25 mM NaH_2PO_4, 25 mM $NaHCO_3$, 20 mM Hepes, 25 mM D-glucose, 12 mM *N*-acetyl-L-cysteine, 5 mM Na ascorbate, 2 mM thiourea, 3 mM Na pyruvate, 3 mM myo-inositol, 0.01 mM taurine, 2 mM $CaCl_2$, and 2 mM $MgSO_4$ (pH 7.2 to 7.3; bubbled with 95% O_2 + 5% CO_2; 300 to 310 mOsm) at room temperature for 15 min. After this recovery period, the slices were maintained at room temperature for at least 30 min before recording in an interface-type holding chamber filled with artificial cerebrospinal fluid (ACSF) containing 119 mM NaCl, 3 mM KCl, 1 mM NaH_2PO_4, 26 mM $NaHCO_3$, 11 mM D-glucose, 0.8 mM Na ascorbate, 2.5 mM $CaCl_2$, and 1.3 mM $MgSO_4$ (pH 7.2 to 7.3; bubbled with 95% O_2 + 5% CO_2; 300 to 310 mOsm). Each slice was transferred to a submersion-type recording chamber (~1 ml) and superfused continuously at a rate of 2 to 3 ml/min with ACSF. All recordings were made at room temperature.

Neurons in the DMH were identified visually using an infrared differential interference contrast (IR-DIC) microscope (BX-51WI, Olympus, Tokyo, Japan) with a water-immersion 40× objective lens (numerical aperture of 0.8). A recording patch pipette (3 to 5 megohms) was filled with the internal solution containing the following: 131 mM CsCl, 10 mM Hepes, 0.2 mM EGTA, 2 mM MgATP, 0.3 mM Na_3GTP, 20 mM phosphocreatine, 2.5 mM QX314 bromide, and 8 mM NaCl (pH 7.2; 295 to 300 mOsm). Biocytin (1 mg/ml) was also added to the internal solution for post hoc fluorescent labeling of recorded neurons. Whole-cell recordings were performed with an EPC-800 amplifier (HEKA, Lambrecht, Germany). Waveform data were digitized at 10 kHz with Digidata 1440A (Molecular Devices, Sunnyvale, CA) and analyzed with pClamp10 (Molecular Devices). Cells were voltage-clamped at −50 mV, and series resistances were 10 to 30 megohms. A train of light pulses (460 nm, 1.5 mW/mm^2, 10-ms duration, and four or five pulses at 20 Hz) was delivered at an interval of 20 s from a blue light-emitting diode (LED) light source (Lambda FLED, Sutter Instruments, Novato, CA) via the objective lens. In some cases, single-pulse stimuli (10-ms duration, 20-s interval) were given. The LED was controlled remotely using transistor-transistor logic pulses from pClamp10. To ensure that synaptic currents were evoked monosynaptically, TTX (0.5 μM) and 4-AP (1 mM) were added to ACSF during recording. After obtaining stable oPSC, we examined the presence of glutamatergic components in the currents by perfusing CNQX (50 μM) and AP5 (50 μM) and then the presence of GABAergic components by perfusing bicuculline (10 μM).

After recordings, the slices were fixed by incubation with 4% formaldehyde in 0.1 M phosphate buffer (pH 7.4) at 4°C overnight. EYFP was immunostained by incubating the slices with an anti-GFP guinea pig antibody (1:5000; 132005, Synaptic Systems), which showed cross-reactivity to EYFP. The slices were then incubated with Alexa488-conjugated goat antibody to guinea pig IgG (5 μg/ml; A11073, Thermo Fisher Scientific) and Alexa647-conjugated streptavidin (2.5 μg/ml; S21374, Thermo Fisher Scientific), the latter of which visualized biocytin. The slices were mounted on glass slides, coverslipped, and observed under a confocal laser scanning microscope (TCS SP8, Leica).

Telemetry monitoring and drug injection in free-moving rats

Surgical procedures followed our previous study (*25*). *Ptger3*-tTA rats were anesthetized with the combination anesthetic described above following gas anesthesia with 3% isoflurane and positioned in a stereotaxic apparatus. After AAV was injected into the POA as described above, a sterile stainless guide cannula (inner diameter = 0.39 mm, outer diameter = 0.71 mm; C313G; Plastic One, Roanoke, VA) was perpendicularly inserted to target the right lateral ventricle (coordinates: 0.8 mm caudal to bregma, 1.8 mm lateral to the midline, and 2.5 mm ventral to the brain surface). The inserted guide cannula was anchored with dental cement to stainless steel screws attached to the skull. A dummy cannula cut to the exact length of the guide cannula was inserted into the guide cannula to avoid clogging. The incisions in the skin were closed with suture, and the wounds were treated with iodine.

One week after the cannulation, the rats were reanesthetized and implanted with a battery-operated telemetric transmitter that projected two cables of external thermistor probes (F40-TT, Data Science International, St. Paul, MN). The transmitter body and one of the thermistor probes to measure T_{core} were placed in the abdominal cavity and sutured to the abdominal wall. The other probe was brought to the back through a tunnel under the skin, inserted into the interscapular BAT pad to measure T_{BAT}, and tied to the fat tissue with suture. We were careful that the whole part of the probe head for T_{BAT} was completely buried into the adipose tissue but was not in contact with the muscle underneath the BAT pad. All the incisions in the abdominal cavity and skin were closed with suture, and the wounds were treated with iodine. After every surgery, the rats were intramuscularly administered with ampicillin sodium and atipamezole hydrochloride. They were housed individually for >1 week to recover from the surgery under regular health check. No rats exhibited any sign of pain or discomfort during the surgical procedures or postoperative recovery. During the recovery period, the rats were habituated to the experimenters and injection procedures once every day.

An internal cannula for injection with the thickness to fit the guide cannula was cut to be long enough to allow the injector tip to protrude 1.0 mm below the tip of the guide cannula. The other end of the internal cannula was connected to a polyethylene tubing whose other end was connected to a Hamilton syringe. The inside of the cannula, tubing, and syringe was filled with pyrogen-free 0.9% saline (Otsuka, Tokyo, Japan) or C21 (200 μg/ml dissolved in saline; SML2392, Sigma-Aldrich). C21 is a potent and selective agonist of hM3Dq and hM4Di and an alternative to the conventional actuator clozapine-*N*-oxide, as C21 has no reported back-metabolism to clozapine in vivo (*29*). The dose of C21 we used was in the range of effective in vivo doses determined in mice (*29*). The rats were lightly anesthetized with isoflurane, the dummy cannula was gently removed, and the internal cannula was inserted into the guide cannula. The solution (5 μl) was ejected into the lateral

ventricle using the syringe at 10:00 a.m. The rats recovered from anesthesia soon after the injection, and T_{core}, T_{BAT}, and activity were monitored with a telemetry system (Data Science International) in a room air-conditioned at 25° ± 1°C. Each rat received saline and C21 injections at an interval of >1 week. After all physiological data acquisition, the rats were transcardially perfused, and expression of the transgene in POA^{EP3R} neurons was immunohistochemically examined as described above. Four rats that were found to lack palGFP or hM3Dq-mCherry expression in POA^{EP3R} neurons, potentially due to off-target AAV injection, were excluded from data analyses.

In some rats, tail skin temperature was measured using a thermal imaging camera (FLIR C2, FLIR). Snapshot thermographic images were taken right before isoflurane anesthesia and 1 hour after saline or C21 injection. FLIR tools plus software was used to acquire skin temperature at 2 to 3 cm from the base of the tail.

In experiments involving PGE_2 injection (Fig. 2A), Sprague-Dawley rats were cannulated in the right lateral ventricle as above and implanted with a telemetric transmitter for T_{core} recording in the abdominal cavity (TA-F40, Data Science International, St. Paul, MN). After a recovery period of >1 week, telemetry monitoring of T_{core} was initiated in a room air-conditioned at 25°C. The rats were lightly anesthetized with isoflurane, and 5 μl of pyrogen-free 0.9% saline or PGE_2 (1 mg/ml dissolved in saline; P5640, Sigma-Aldrich) was injected into the lateral ventricle through the cannula as mentioned above. The rats quickly recovered from anesthesia, and 10 min after the injection, they were placed in a climate chamber air-conditioned at 36°C. After monitoring of their T_{core} in the chamber for 75 min, the rats were immediately anesthetized and transcardially perfused as above.

In vivo electrophysiology in anesthetized rats

In vivo physiological recordings followed our established procedure (*11*, *24*). *Ptger3*-tTA rats that had recovered from surgery for AAV injections into the POA were anesthetized intravenously with urethane (0.8 g/kg) and α-chloralose (80 mg/kg) after cannulation of a femoral artery, a femoral vein, and the trachea under anesthesia with 3% isoflurane in 100% O_2. They were then placed in a stereotaxic apparatus, and the arterial cannula was attached to a pressure transducer to record arterial pressure and HR. T_{core} was monitored from the rectum and maintained at 36.0° to 38.0°C by perfusing a plastic water jacket, which was wrapped around the shaved trunk, with warm or cold water. The animal was then artificially ventilated with 100% O_2 through the tracheal cannula and paralyzed with D-tubocurarine (0.6 mg, iv, initial dose, supplemented with 0.3 mg/hour) to stabilize BAT nerve recording by preventing respiration-related movements. Every time the effect of tubocurarine waned, the depth of anesthesia was reassessed before supplementation of tubocurarine, and the anesthetic was supplemented as necessary. Mixed expired CO_2 was monitored through the tracheal cannula using a capnometer to provide an index of changes in whole-body metabolism and was maintained at 3.5 to 4.5% under basal conditions. T_{BAT} was measured from the left interscapular BAT pad, and postganglionic BAT SNA was recorded from the central cut end of a nerve bundle isolated from the right interscapular BAT pad.

BAT SNA was amplified (×5000 to 10,000) and filtered (1 to 300 Hz) using a CyberAmp 380 amplifier (Molecular Devices). All the physiological variables were digitized and recorded to a personal computer using Spike2 software (version 7.10; CED, Cambridge, UK). For nanoinjection of drugs, a sharp glass pipette (tip inner diameter: 15 to 30 μm) filled with NMDA (0.2 mM; Sigma-Aldrich, M3262), C21 (200 μg/ml), or pyrogen-free 0.9% saline was perpendicularly inserted into the DMH and pressure-ejected (50 nl for unilateral injection and 100 nl per site for bilateral C21 injections). All drugs were dissolved in pyrogen-free 0.9% saline. To identify the injection site, a small amount (~5 nl) of 0.2% FluoSpheres (0.1 μm diameter, 0.2% solids in saline; F8801 or F8803, Thermo Fisher Scientific) was injected at the same site with the same pipette at the end of recordings.

For data analyses in Fig. 7E and Table 1, BAT SNA amplitudes were quantified using Spike2 in sequential 4-s bins as the square root of the total power (root mean square) in the 0- to 20-Hz band of the autospectra of each 4-s segment of the BAT SNA traces. The "power/4-s" traces (Fig. 7, B to D) were used for quantification and statistical analyses of changes in BAT SNA. In Fig. 7E, baseline values of BAT SNA, T_{BAT}, expired CO_2, HR, and mean arterial pressure were the averages during the 1-min period immediately before NMDA injection. NMDA-evoked changes in T_{BAT}, expired CO_2, HR, and mean arterial pressure were the differences between their baseline values and their peak values within 5 min (10 min for T_{BAT}) after NMDA injection. NMDA-evoked changes in BAT SNA were the area under the curve (AUC) of the power/4-s trace above the baseline level (subtracted AUC) for 5 min after NMDA injection. NMDA-evoked increases in subtracted AUC following C21 injection into the DMH were expressed as % of NMDA-evoked increases in subtracted AUC following saline injection (ΔBAT SNA; Fig. 7E).

Table 1 compares physiological variables before and after bilateral C21 injections into the DMH (Fig. 7B). Preinjection (baseline) values of T_{BAT}, expired CO_2, HR, and mean arterial pressure were the averages during the 1-min period immediately before the first C21 injection. Postinjection values of T_{BAT}, expired CO_2, HR, and mean arterial pressure were their peak values within 5 min after completion of bilateral C21 injections. Postinjection BAT SNA was the average of the power/4-s value for 5 min after completion of C21 injections and expressed as % of the baseline value during the preinjection 1-min period.

Anatomy and statistical analysis

We adopted the cytoarchitecture and nomenclature of most brain regions from those of Paxinos and Watson (*64*). The DMH consisted of the dorsomedial hypothalamic nucleus and dorsal hypothalamic area (Fig. 4C) (*13*, *25*). The raphe pallidus nucleus was nomenclaturally divided into the rostral (rRPa) and caudal (cRPa) parts at the rostral end of the inferior olivary complex (fig. S5, J and K) (*10*, *23*).

Data are shown as the means ± SEM. Statistic comparison analyses were performed using a paired or unpaired *t* test, an ordinary or repeated-measures one-way analysis of variance (ANOVA) followed by Bonferroni's multiple comparisons test, or a repeated-measures two-way ANOVA followed by Bonferroni's multiple comparisons test (Prism 9, GraphPad) as stated in the text and figure legends. All the statistic tests were two-sided. $P < 0.05$ was considered statistically significant.

Correction (3 May 2023): Due to a production, the incorrect version of the supplemental PDF was used for publication. In the left column of table S1, the previous version erroneously stated

that the data supported figure S6 in the supplementary materials. The supplemental PDF has now been corrected and shows that the data from this table supports Figure 6 in the main text.

Supplementary Materials

This PDF file includes:
Figs. S1 to S7
Table S1

View/request a protocol for this paper from *Bio-protocol*.

REFERENCES AND NOTES

1. K. Nakamura, Central circuitries for body temperature regulation and fever. *Am. J. Physiol. Regul. Integr. Comp. Physiol.* **301**, R1207–R1228 (2011).
2. C. L. Tan, Z. A. Knight, Regulation of body temperature by the nervous system. *Neuron* **98**, 31–48 (2018).
3. S. F. Morrison, K. Nakamura, Central mechanisms for thermoregulation. *Annu. Rev. Physiol.* **81**, 285–308 (2019).
4. K. Nakamura, Y. Nakamura, N. Kataoka, A hypothalamomedullary network for physiological responses to environmental stresses. *Nat. Rev. Neurosci.* **23**, 35–52 (2022).
5. K. Yamagata, K. Matsumura, W. Inoue, T. Shiraki, K. Suzuki, S. Yasuda, H. Sugiura, C. Cao, Y. Watanabe, S. Kobayashi, Coexpression of microsomal-type prostaglandin E synthase with cyclooxygenase-2 in brain endothelial cells of rats during endotoxin-induced fever. *J. Neurosci.* **21**, 2669–2677 (2001).
6. K. Nakamura, S. F. Morrison, A thermosensory pathway that controls body temperature. *Nat. Neurosci.* **11**, 62–71 (2008).
7. K. Nakamura, S. F. Morrison, A thermosensory pathway mediating heat-defense responses. *Proc. Natl. Acad. Sci. U.S.A.* **107**, 8848–8853 (2010).
8. X. M. Chen, T. Hosono, T. Yoda, Y. Fukuda, K. Kanosue, Efferent projection from the preoptic area for the control of non-shivering thermogenesis in rats. *J. Physiol.* **512**, 883–892 (1998).
9. J. A. Rathner, C. J. Madden, S. F. Morrison, Central pathway for spontaneous and prostaglandin E_2-evoked cutaneous vasoconstriction. *Am. J. Physiol. Regul. Integr. Comp. Physiol.* **295**, R343–R354 (2008).
10. K. Nakamura, K. Matsumura, T. Kaneko, S. Kobayashi, H. Katoh, M. Negishi, The rostral raphe pallidus nucleus mediates pyrogenic transmission from the preoptic area. *J. Neurosci.* **22**, 4600–4610 (2002).
11. K. Nakamura, S. F. Morrison, Central efferent pathways for cold-defensive and febrile shivering. *J. Physiol.* **589**, 3641–3658 (2011).
12. Y. Nakamura, K. Nakamura, K. Matsumura, S. Kobayashi, T. Kaneko, S. F. Morrison, Direct pyrogenic input from prostaglandin EP3 receptor-expressing preoptic neurons to the dorsomedial hypothalamus. *Eur. J. Neurosci.* **22**, 3137–3146 (2005).
13. Y. Nakamura, K. Nakamura, S. F. Morrison, Different populations of prostaglandin EP3 receptor-expressing preoptic neurons project to two fever-mediating sympathoexcitatory brain regions. *Neuroscience* **161**, 614–620 (2009).
14. K. Nakamura, T. Kaneko, Y. Yamashita, H. Hasegawa, H. Katoh, A. Ichikawa, M. Negishi, Immunocytochemical localization of prostaglandin EP3 receptor in the rat hypothalamus. *Neurosci. Lett.* **260**, 117–120 (1999).
15. K. Nakamura, T. Kaneko, Y. Yamashita, H. Hasegawa, H. Katoh, M. Negishi, Immunohistochemical localization of prostaglandin EP3 receptor in the rat nervous system. *J. Comp. Neurol.* **421**, 543–569 (2000).
16. M. Lazarus, K. Yoshida, R. Coppari, C. E. Bass, T. Mochizuki, B. B. Lowell, C. B. Saper, EP3 prostaglandin receptors in the median preoptic nucleus are critical for fever responses. *Nat. Neurosci.* **10**, 1131–1133 (2007).
17. N. Machado, S. S. Bandaru, S. Abbott, C. B. Saper, EP3R-expressing glutamatergic preoptic neurons mediate inflammatory fever. *J. Neurosci.* **40**, 2573–2588 (2020).
18. S. Narumiya, Y. Sugimoto, F. Ushikubi, Prostanoid receptors: Structures, properties, and functions. *Physiol. Rev.* **79**, 1193–1226 (1999).
19. K. Moriyoshi, L. J. Richards, C. Akazawa, D. D. M. O'Leary, S. Nakanishi, Labeling neural cells using adenoviral gene transfer of membrane-targeted GFP. *Neuron* **16**, 255–260 (1996).
20. T. Kaneko, F. Fujiyama, Complementary distribution of vesicular glutamate transporters in the central nervous system. *Neurosci. Res.* **42**, 243–250 (2002).
21. M. V. Zaretskaia, D. V. Zaretsky, J. A. DiMicco, Role of the dorsomedial hypothalamus in thermogenesis and tachycardia caused by microinjection of prostaglandin E2 into the preoptic area in anesthetized rats. *Neurosci. Lett.* **340**, 1–4 (2003).
22. C. J. Madden, S. F. Morrison, Excitatory amino acid receptors in the dorsomedial hypothalamus mediate prostaglandin-evoked thermogenesis in brown adipose tissue. *Am. J. Physiol. Regul. Integr. Comp. Physiol.* **286**, R320–R325 (2004).
23. K. Nakamura, K. Matsumura, T. Hübschle, Y. Nakamura, H. Hioki, F. Fujiyama, Z. Boldogköi, M. König, H.-J. Thiel, R. Gerstberger, S. Kobayashi, T. Kaneko, Identification of sympathetic premotor neurons in medullary raphe regions mediating fever and other thermoregulatory functions. *J. Neurosci.* **24**, 5370–5380 (2004).
24. K. Nakamura, S. F. Morrison, Central efferent pathways mediating skin cooling-evoked sympathetic thermogenesis in brown adipose tissue. *Am. J. Physiol. Regul. Integr. Comp. Physiol.* **292**, R127–R136 (2007).
25. N. Kataoka, H. Hioki, T. Kaneko, K. Nakamura, Psychological stress activates a dorsomedial hypothalamus-medullary raphe circuit driving brown adipose tissue thermogenesis and hyperthermia. *Cell Metab.* **20**, 346–358 (2014).
26. B. C. Samuels, D. V. Zaretsky, J. A. DiMicco, Dorsomedial hypothalamic sites where disinhibition evokes tachycardia correlate with location of raphe-projecting neurons. *Am. J. Physiol. Regul. Integr. Comp. Physiol.* **287**, R472–R478 (2004).
27. B. L. Roth, DREADDs for neuroscientists. *Neuron* **89**, 683–694 (2016).
28. T. J. Stachniak, A. Ghosh, S. M. Sternson, Chemogenetic synaptic silencing of neural circuits localizes a hypothalamus→midbrain pathway for feeding behavior. *Neuron* **82**, 797–808 (2014).
29. K. J. Thompson, E. Khajehali, S. J. Bradley, J. S. Navarrete, X. P. Huang, S. Slocum, J. Jin, J. Liu, Y. Xiong, R. H. J. Olsen, J. F. Diberto, K. M. Boyt, M. M. Pina, D. Pati, C. Molloy, C. Bundgaard, P. M. Sexton, T. L. Kash, M. J. Krashes, A. Christopoulos, B. L. Roth, A. B. Tobin, DREADD agonist 21 is an effective agonist for muscarinic-based DREADDs *in vitro* and *in vivo*. *ACS Pharmacol. Transl. Sci.* **1**, 61–72 (2018).
30. M. Tanaka, M. J. McKinley, R. M. McAllen, Preoptic-raphé connections for thermoregulatory vasomotor control. *J. Neurosci.* **31**, 5078–5088 (2011).
31. E. P. S. da Conceição, S. F. Morrison, G. Cano, P. Chiavetta, D. Tupone, Median preoptic area neurons are required for the cooling and febrile activations of brown adipose tissue thermogenesis in rat. *Sci. Rep.* **10**, 18072 (2020).
32. R. A. Piñol, A. S. Mogul, C. K. Hadley, A. Saha, C. Li, V. Škop, H. S. Province, C. Xiao, O. Gavrilova, M. J. Krashes, M. L. Reitman, Preoptic BRS3 neurons increase body temperature and heart rate via multiple pathways. *Cell Metab.* **33**, 1389–1403.e6 (2021).
33. J. A. Boulant, Role of the preoptic-anterior hypothalamus in thermoregulation and fever. *Clin. Infect. Dis.* **31**,**Suppl 5**, S157–S161 (2000).
34. K. Song, H. Wang, G. B. Kamm, J. Pohle, F. C. Reis, P. Heppenstall, H. Wende, J. Siemens, The TRPM2 channel is a hypothalamic heat sensor that limits fever and can drive hypothermia. *Science* **353**, 1393–1398 (2016).
35. S. Yu, E. Qualls-Creekmore, K. Rezai-Zadeh, Y. Jiang, H. R. Berthoud, C. D. Morrison, A. V. Derbenev, A. Zsombok, H. Münzberg, Glutamatergic preoptic area neurons that express leptin receptors drive temperature-dependent body weight homeostasis. *J. Neurosci.* **36**, 5034–5046 (2016).
36. S. B. G. Abbott, C. B. Saper, Median preoptic glutamatergic neurons promote thermoregulatory heat loss and water consumption in mice. *J. Physiol.* **595**, 6569–6583 (2017).
37. Z.-D. Zhao, W. Z. Yang, C. Gao, X. Fu, W. Zhang, Q. Zhou, W. Chen, X. Ni, J. K. Lin, J. Yang, X.-H. Xu, W. L. Shen, A hypothalamic circuit that controls body temperature. *Proc. Natl. Acad. Sci. U.S.A.* **114**, 2042–2047 (2017).
38. C. L. Tan, E. K. Cooke, D. E. Leib, Y.-C. Lin, G. E. Daly, C. A. Zimmerman, Z. A. Knight, Warm-sensitive neurons that control body temperature. *Cell* **167**, 47–59.e15 (2016).
39. E. C. Harding, X. Yu, A. Miao, N. Andrews, Y. Ma, Z. Ye, L. Lignos, G. Miracca, W. Ba, R. Yustos, A. L. Vyssotski, W. Wisden, N. P. Franks, A neuronal hub binding sleep initiation and body cooling in response to a warm external stimulus. *Curr. Biol.* **28**, 2263–2273.e4 (2018).
40. D. Kroeger, G. Absi, C. Gagliardi, S. S. Bandaru, J. C. Madara, L. L. Ferrari, E. Arrigoni, H. Münzberg, T. E. Scammell, C. B. Saper, R. Vetrivelan, Galanin neurons in the ventrolateral preoptic area promote sleep and heat loss in mice. *Nat. Commun.* **9**, 4129 (2018).
41. Y. Ma, G. Miracca, X. Yu, E. C. Harding, A. Miao, R. Yustos, A. L. Vyssotski, N. P. Franks, W. Wisden, Galanin neurons unite sleep homeostasis and α2-adrenergic sedation. *Curr. Biol.* **29**, 3315–3322.e3 (2019).
42. S. Hrvatin, S. Sun, O. F. Wilcox, H. Yao, A. J. Lavin-Peter, M. Cicconet, E. G. Assad, M. E. Palmer, S. Aronson, A. S. Banks, E. C. Griffith, M. E. Greenberg, Neurons that regulate mouse torpor. *Nature* **583**, 115–121 (2020).
43. T. M. Takahashi, G. A. Sunagawa, S. Soya, M. Abe, K. Sakurai, K. Ishikawa, M. Yanagisawa, H. Hama, E. Hasegawa, A. Miyawaki, K. Sakimura, M. Takahashi, T. Sakurai, A discrete neuronal circuit induces a hibernation-like state in rodents. *Nature* **583**, 109–114 (2020).
44. K. X. Zhang, S. D'Souza, B. A. Upton, S. Kernodle, S. Vemaraju, G. Nayak, K. D. Gaitonde, A. L. Holt, C. D. Linne, A. N. Smith, N. T. Petts, M. Batie, R. Mukherjee, D. Tiwari, E. D. Buhr, R. N. Van Gelder, C. Gross, A. Sweeney, J. Sanchez-Gurmaches, R. J. Seeley, R. A. Lang, Violet-light suppression of thermogenesis by opsin 5 hypothalamic neurons. *Nature* **585**, 420–425 (2020).
45. Z. Zhang, F. M. C. V. Reis, Y. He, J. W. Park, J. R. DiVittorio, N. Sivakumar, J. E. van Veen, S. Maesta-Pereira, M. Shum, I. Nichols, M. G. Massa, S. Anderson, K. Paul, M. Liesa,

O. A. Ajijola, Y. Xu, A. Adhikari, S. M. Correa, Estrogen-sensitive medial preoptic area neurons coordinate torpor in mice. *Nat. Commun.* **11**, 6378 (2020).
46. J. A. Osterhout, V. Kapoor, S. W. Eichhorn, E. Vaughn, J. D. Moore, D. Liu, D. Lee, L. A. DeNardo, L. Luo, X. Zhuang, C. Dulac, A preoptic neuronal population controls fever and appetite during sickness. *Nature* **606**, 937–944 (2022).
47. M. Sheng, G. McFadden, M. E. Greenberg, Membrane depolarization and calcium induce c-fos transcription via phosphorylation of transcription factor CREB. *Neuron* **4**, 571–582 (1990).
48. T. Nakayama, J. S. Eisenman, J. D. Hardy, Single unit activity of anterior hypothalamus during local heating. *Science* **134**, 560–561 (1961).
49. P. A. Mackowiak, J. A. Boulant, Fever's glass ceiling. *Clin. Infect. Dis.* **22**, 525–536 (1996).
50. A. A. Steiner, J. Antunes-Rodrigues, L. G. S. Branco, Role of preoptic second messenger systems (cAMP and cGMP) in the febrile response. *Brain Res.* **944**, 135–145 (2002).
51. N. Kataoka, Y. Shima, K. Nakajima, K. Nakamura, A central master driver of psychosocial stress responses in the rat. *Science* **367**, 1105–1112 (2020).
52. J. R. Moffitt, D. Bambah-Mukku, S. W. Eichhorn, E. Vaughn, K. Shekhar, J. D. Perez, N. D. Rubinstein, J. Hao, A. Regev, C. Dulac, X. Zhuang, Molecular, spatial, and functional single-cell profiling of the hypothalamic preoptic region. *Science* **362**, eaau5324 (2018).
53. B. A. Upton, S. P. D'Souza, R. A. Lang, QPLOT neurons-converging on a thermoregulatory preoptic neuronal population. *Front. Neurosci.* **15**, 665762 (2021).
54. Y. Liu, A. Beyer, R. Aebersold, On the dependency of cellular protein levels on mRNA abundance. *Cell* **165**, 535–550 (2016).
55. H. Jung, B. C. Yoon, C. E. Holt, Axonal mRNA localization and local protein synthesis in nervous system assembly, maintenance and repair. *Nat. Rev. Neurosci.* **13**, 308–324 (2012).
56. C. E. Holt, K. C. Martin, E. M. Schuman, Local translation in neurons: Visualization and function. *Nat. Struct. Mol. Biol.* **26**, 557–566 (2019).
57. M. Takahashi, Y. Ishida, N. Kataoka, K. Nakamura, H. Hioki, Efficient labeling of neurons and identification of postsynaptic sites using adeno-associated virus vector, in *Receptor and Ion Channel Detection in the Brain*, R. Lujan, F. Ciruela, Eds., vol. 169 of *Neuromethods* (Humana Press, ed. 2, 2021), pp. 323–341.
58. H. Hioki, E. Kuramoto, M. Konno, H. Kameda, Y. Takahashi, T. Nakano, K. C. Nakamura, T. Kaneko, High-level transgene expression in neurons by lentivirus with Tet-Off system. *Neurosci. Res.* **63**, 149–154 (2009).
59. J. Sohn, M. Takahashi, S. Okamoto, Y. Ishida, T. Furuta, H. Hioki, A single vector platform for high-level gene transduction of central neurons: Adeno-associated virus vector equipped with the Tet-Off system. *PLOS ONE* **12**, e0169611 (2017).
60. N. Tamamaki, K. Nakamura, T. Furuta, K. Asamoto, T. Kaneko, Neurons in Golgi-stain-like images revealed by GFP-adenovirus infection in vivo. *Neurosci. Res.* **38**, 231–236 (2000).
61. H. Hioki, F. Fujiyama, K. Taki, R. Tomioka, T. Furuta, N. Tamamaki, T. Kaneko, Differential distribution of vesicular glutamate transporters in the rat cerebellar cortex. *Neuroscience* **117**, 1–6 (2003).
62. H. Hioki, H. Nakamura, Y. F. Ma, M. Konno, T. Hayakawa, K. C. Nakamura, F. Fujiyama, T. Kaneko, Vesicular glutamate transporter 3-expressing nonserotonergic projection neurons constitute a subregion in the rat midbrain raphe nuclei. *J. Comp. Neurol.* **518**, 668–686 (2010).
63. K. Nakamura, A. Watakabe, H. Hioki, F. Fujiyama, Y. Tanaka, T. Yamamori, T. Kaneko, Transiently increased colocalization of vesicular glutamate transporters 1 and 2 at single axon terminals during postnatal development of mouse neocortex: A quantitative analysis with correlation coefficient. *Eur. J. Neurosci.* **26**, 3054–3067 (2007).
64. G. Paxinos, C. Watson, *The Rat Brain in Stereotaxic Coordinates* (Academic Press, ed. 6, 2007).

Acknowledgments: We thank A. Watakabe for sharing the VGLUT2 antisense probe; K. Deisseroth, B. Roth, S. Sternson, and W. Wisden for sharing plasmids; M. Takemoto for technical assistance for AAV production; S. F. Morrison for critical reading of the manuscript; and T. Kaneko for helpful discussion. **Funding:** This study was supported by the Funding Program for Next Generation World-Leading Researchers from the Japan Society for the Promotion of Science (LS070 to K.N.); Grants-in-Aid for Scientific Research [JP21K06767, JP17K08568, JP26860159, and JP23790271 to Y.N.; JP22K06844 to A.F.; JP22K06470, JP19K06954, and JP16K19006 to N.K.; JP21H02592 to H.H.; JP20H03418, JP16H06276 (AdAMS), JP16H05128, JP15H05932, JP26118508, JP26713009, and JP22689007 to K.N.] from the Ministry of Education, Culture, Sports, Science and Technology of Japan; the PRESTO program (JPMJPR13M9 to K.N.), the FOREST program (JPMJFR204D to H.H.), and Moonshot R&D (JPMJMS2024 to H.H. and JPMJMS2023 to K.N.) of the Japan Science and Technology Agency; the Japan Agency for Medical Research and Development (JP21wm0525002 to N.K., JP21dm0207112 to H.H., and JP21gm5010002 to K.N.); grants from the Hori Sciences and Arts Foundation (to Y.N.); the Kato Memorial Bioscience Foundation and the Foundation of Kinoshita Memorial Enterprise (to N.K.); and the Takeda Science Foundation, Nakajima Foundation, Uehara Memorial Foundation, Ono Medical Research Foundation, Brain Science Foundation, Kowa Life Science Foundation, and Nagoya University Research Fund (to K.N.). T.Y. is supported by the Takeda Science Foundation scholarship. The maintenance of the *Ptger3-tTA* transgenic rat strain was supported by the National BioResource Project–Rat, Kyoto University and by the Center for Animal Research and Education, Nagoya University. **Author contributions:** Y.N. and K.N. designed experiments. Y.N., T.Y., A.F., and K.N. performed experiments and analyzed and discussed data. Y.N., H.H., and K.N. generated and supplied *Ptger3-tTA* transgenic rats. N.K., H.H., and K.N. generated AAVs. Y.N. and K.N. wrote the manuscript, and all authors approved the manuscript. **Competing interests:** The authors declare that they have no competing interests. **Data and materials availability:** All data needed to evaluate the conclusions in the paper are present in the paper and/or the Supplementary Materials. *Ptger3*-tTA rats can be provided by the corresponding author pending scientific review and a completed material transfer agreement. Requests for *Ptger3*-tTA rats should be submitted to the corresponding author.

Submitted 17 June 2022
Accepted 8 November 2022
Published 23 December 2022
10.1126/sciadv.add5463